AIP | The Journal of Chemical Physics

Dynamic processes in a silicate liquid from above melting to below the glass transition

Marcio Luis Ferreira Nascimento, Vladimir Mihailovich Fokin, Edgar Dutra Zanotto, and Alexander S. Abyzov

Citation: J. Chem. Phys. **135**, 194703 (2011); doi: 10.1063/1.3656696
View online: http://dx.doi.org/10.1063/1.3656696
View Table of Contents: http://jcp.aip.org/resource/1/JCPSA6/v135/i19
Published by the American Institute of Physics.

Dynamic processes in a silicate liquid from above melting to below the glass transition

Marcio Luis Ferreira Nascimento,[1] Vladimir Mihailovich Fokin,[2,a)] Edgar Dutra Zanotto,[3,b)] and Alexander S. Abyzov[4]

[1]*Institute of Humanities, Arts & Sciences, Federal University of Bahia, Rua Barão de Jeremoabo s/n, Glauber Rocha Pavilion (PAF 3), Ondina University Campus, 40170-115 Salvador-BA, Brazil*
[2]*Vavilov State Optical Institute, ul. Babushkina 36-1, 193171 St. Petersburg, Russia*
[3]*Vitreous Materials Laboratory, Department of Materials Engineering, Federal University of São Carlos 13595-905, São Carlos-SP, Brazil*
[4]*National Science Center, Kharkov Institute of Physics and Technology, Academician Street 1, 61108 Kharkov, Ukraine*

(Received 15 July 2011; accepted 9 October 2011; published online 17 November 2011)

We collect and critically analyze extensive literature data, including our own, on three important kinetic processes—viscous flow, crystal nucleation, and growth—in lithium disilicate ($Li_2O \cdot 2SiO_2$) over a wide temperature range, from above T_m to $0.98T_g$ where $T_g \approx 727$ K is the calorimetric glass transition temperature and $T_m = 1307$ K, which is the melting point. We found that crystal growth mediated by screw dislocations is the most likely growth mechanism in this system. We then calculated the diffusion coefficients controlling crystal growth, D^U_{eff}, and completed the analyses by looking at the ionic diffusion coefficients of Li^{+1}, O^{2-}, and Si^{4+} estimated from experiments and molecular dynamic simulations. These values were then employed to estimate the effective volume diffusion coefficients, D^V_{eff}, resulting from their combination within a hypothetical $Li_2Si_2O_5$ "molecule". The similarity of the temperature dependencies of $1/\eta$, where η is shear viscosity, and D^V_{eff} corroborates the validity of the Stokes-Einstein/Eyring equation (SEE) at high temperatures around T_m. Using the equality of D^V_{eff} and D^η_{eff}, we estimated the jump distance $\lambda \sim 2.70$ Å from the SEE equation and showed that the values of D^U_{eff} have the same temperature dependence but exceed D^η_{eff} by about eightfold. The difference between D^η_{eff} and D^U_{eff} indicates that the former determines the process of mass transport in the bulk whereas the latter relates to the mobility of the structural units on the crystal/liquid interface. We then employed the values of $\eta(T)$ reduced by eightfold to calculate the growth rates $U(T)$. The resultant $U(T)$ curve is consistent with experimental data until the temperature decreases to a decoupling temperature $T^U_d \approx 1.1 - 1.2T_g$, when D^η_{eff} begins decrease with decreasing temperature faster than D^U_{eff}. A similar decoupling occurs between D^η_{eff} and D^τ_{eff} (estimated from nucleation time-lags) but at a lower temperature$T^\tau_d \approx T_g$. For $T > T_g$ the values of D^τ_{eff} exceed D^η_{eff} only by twofold. The different behaviors of $D^\tau_{eff}(T)$ and $D^U_{eff}(T)$ are likely caused by differences in the mechanisms of critical nuclei formation. Therefore, we have shown that at low undercoolings, viscosity data can be employed for quantitative analyses of crystal growth rates, but in the deeply supercooled liquid state, mass transport for crystal nucleation and growth are not controlled by viscosity. The origin of decoupling is assigned to spatially *dynamic heterogeneity* in glass-forming melts. © *2011 American Institute of Physics*. [doi:10.1063/1.3656696]

I. INTRODUCTION

The kinetics and mechanisms of crystallization in undercooled liquids are key issues in several important fields. For instance, pharmacists, chemists and chemical engineers strongly depend upon controlled crystallization for the synthesis of numerous organic and inorganic compounds, and geologists often rely on "post-mortem" analyses of crystallization to understand the formation of minerals and solidified magmas. Switching between glassy and crystalline states in phase-change thin films is presently exploited for data storage. Crystallization of vitreous materials can lead to a wide range of *glass-ceramics* (high tech polycrystalline materials prepared by the controlled crystallization of glasses) having unusual microstructures and properties.[1] Moreover, the glassy state is only attainable when the thermodynamically favorable path—crystallization—is avoided when cooling a melt. From a more fundamental point of view, glasses are a convenient object to study various aspects of crystal nucleation and growth. As was figuratively mentioned in Refs. 2 and 3, glasses are the "*Drosophila of nucleation theory*". Thus, from both theoretical and practical points of view, it is important to understand and control the kinetics and mechanisms of

a)Author to whom correspondence should be addressed. Electronic mail: vmfokin@gmail.com.
b)URL: www.lamav.weebly.com.

crystal nucleation and growth in undercooled glass-forming liquids.

Lithium disilicate $Li_2O \cdot 2SiO_2$ (LS_2) was the first inorganic glass for which internal crystal nucleation rates were measured, which took place more than 40 years ago.[4,5] Since that time, this glass has been employed as a popular "model" system. In addition, lithium silicate is the basis for several commercial glass-ceramics; therefore, a plethora of experimental data has been obtained for this glass.

The present work deals with two interconnected topics. In the first, we collect, combine, analyze, and discuss literature data (including our own) on several dynamic processes in LS_2 liquid, such as *viscous flow*,[6–34] *crystal nucleation*,[30–34,36–43] *crystal growth*,[20–29,32–36] *ionic conductivity*[44–57] and *ionic self-diffusion*.[58–61] These processes are explored over a very wide temperature range—from temperatures slightly below the glass transition temperature, T_g, up to temperatures above melting point, T_m. This data array is quite impressive; it suffices to mention that the total number of (difficult-to-measure) kinetic data points is about 500. In conclusion, the first part of the paper focuses on an analysis of published data and a *critical* review of dynamic processes in LS_2 glass.

In the second part, this rich data array allowed us to perform a comparative analysis of diffusivity in connection with viscous flow, crystallization, and especially with a general problem, i.e., the possible breakdown of the Stokes-Einstein/Eyring equation, which has been documented and investigated for different undercooled glass forming systems, such as inorganic and metallic glasses, polymers, and organic liquids, see, e.g., Refs. 62–67. The breakdown of the SEE equation has been assigned to the change of molecular motion from a liquid-like (at temperatures close to the liquidus) to a very viscous behavior at lower temperatures that is associated to the evolution of spatially heterogeneous dynamics, as suggested by theoretical and simulation work.[68] In the present analysis we employed crystal growth rates and also nucleation data (for the first time) to estimate the effective diffusion coefficients and to compare them with the self-diffusion coefficients of ionic species Si^{4+}, O^{2-}, and Li^{+} estimated from real experiments and calculated by molecular dynamic (MD) simulations. Available thermodynamic data for LS_2 crystals, glass and liquid facilitate this analysis. The second part is thus aimed to shed light into the ionic species controlling crystallization and viscous flow in this "model" undercooled silicate glass forming liquid.

II. LITERATURE DATA

We present below most of the literature results we found on viscous flow, crystal nucleation, crystal growth, ionic conductivity, and ionic diffusivity of Li^{+}, O^{2-}, and Si^{4+} for this particular system. We only discarded data that were clearly in error and unusual for each process of interest.

A. Viscosity

Viscosity is one of the most important properties of glass-forming melts, but its theoretical treatment is still a great challenge for glass-forming liquids. Briefly speaking, the main problem is the lack of knowledge about the "flow units" constituting viscous flow, how the liquid structure changes with temperature, and how such structural changes influence the flow units. In certain temperature ranges, glass-forming melts probably possess a more or less fixed flow unit type/size and, thus, behave as a "quasi-molecular" fluid, a fact that encompasses the applicability of the Stokes-Einstein/Eyring (SEE) equation, described below. Fortunately, available viscosity data for LS_2 span about twelve orders of magnitude[6–34] in the temperature range 450–1450 °C, i.e., from DSC-T_g to well above T_m, and will be thoroughly used in this paper.

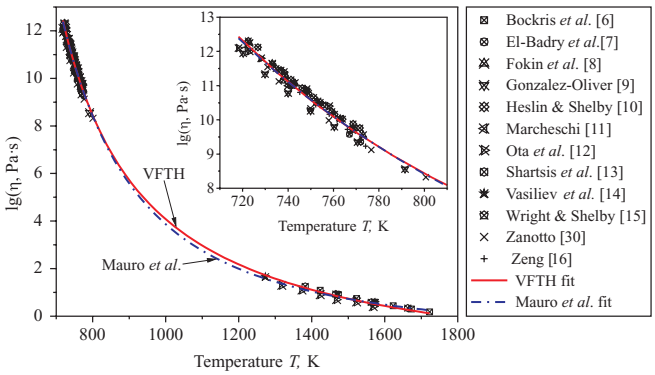

FIG. 1. Selected viscosity data (Refs. 6–16 and 30) obtained by different techniques for different lithium disilicate glasses reported in Refs. 6–34 plus results of fittings by the following equations: VFTH (with $A = -2.662$, $B = 3432.54$ K, and $T_0 = 490.71$ K) and by the MYEGA, Mauro *et al.*, (Ref. 75) with $A = -2.662$, $T_g = 724.81$ K, and $m = 45.4$). The inset shows magnified details at low temperatures near T_g.

Fig. 1 shows selected viscosity data[6–16,30] for several lithium disilicate glasses reported by different authors. Ota *et al.*[12] used the penetration, beam-bending and counterbalance methods between 1 and 10^{12} Pa s. Matusita and Tashiro[31] and Matusita *et al.*[19] presented the lowest viscosity values ever measured for this glass by beam-bending and penetration techniques in the range of 450 °C–536 °C, with no indication of water content or chemical analysis. In fact, Matusita *et al.*[19] measured viscosity for another glass batch under argon atmosphere and obtained a value for the glass transition temperature, $T_g = 447$ °C, that is lower than the expected value ($T_g \approx 454$ °C by DSC at 10 K/min) from the majority of authors. Heslin and Shelby[10] measured the viscosity of two batches of LS_2 glass melted at 1400 °C for 5h in dry and wet flowing air atmospheres. Infrared absorption spectra of wet and dry glasses show that the wet glass contained approximately six times the water content of the dry glass (no assessment of the OH^{-} amounts for each batch were given), and the temperature difference at the 10^{12} Pa s isokom was 10 °C. We discarded the measurements for the dry glass from our analysis because they showed the highest viscosity values measured, while the wet glass was considered a glass with typical OH^{-} content and presented common viscosity values. Vasiliev and Lisenenkov[14]measured viscosity in a rotating viscosimeter using a molybdenum crucible. Izumitani and Moriya[17] and El-Badry *et al.*[7] used the fiber elongation method, with no indication of the chemical analysis. Shartsis *et al.*[13] used the counterbalanced method with Pt body and crucible and analyzed alkali content samples

by evaporation to dryness on a steam bath with HF to the corresponding fluorosilicate. They also measured and compared density data and found similar results to the literature. Zeng,[16] Zanotto,[30] Gonzalez-Oliver,[9] Marcheschi[11] and Joseph[18] used the beam-bending method, while Bockris *et al.*[6] used a rotating viscosimeter with a molybdenum body and crucible. Bockris *et al.*[6] affirmed that all of their melts were analyzed after the experiments and that the average deviation between the calculated and analyzed compositions was less than 0.5%. Marcheschi[11] did not present the chemical analysis but measured T_g by DSC at 20 K/min, obtaining 460 °C, which is a reasonable result for this heating rate. Zanotto[30] and Gonzalez-Oliver[9] performed flame photometry measurements and found results close to the stoichiometric composition. Fokin *et al.*[8] used the viscosity data of V. P. Kluyev obtained by the beam-bending method.

Out of all of the available data,[6–34] we only excluded some marginal points, e.g., the lowest viscosity (from Matusita *et al.*[19] and Matusita and Tashiro[31]) and the highest viscosities (from Izumitani and Moriya[17] and Heslin and Shelby's "dry glass"[10]). The significant difference between the above-mentioned data and other authors' data could be caused by measurement errors, significant deviations in the compositions or different water contents. All of these issues can seriously affect viscosity, as illustrated in Fig. 2 (see also Ref. 69). By discarding the extreme data, we guaranteed some confidence in the composition similarity of the selected glasses.

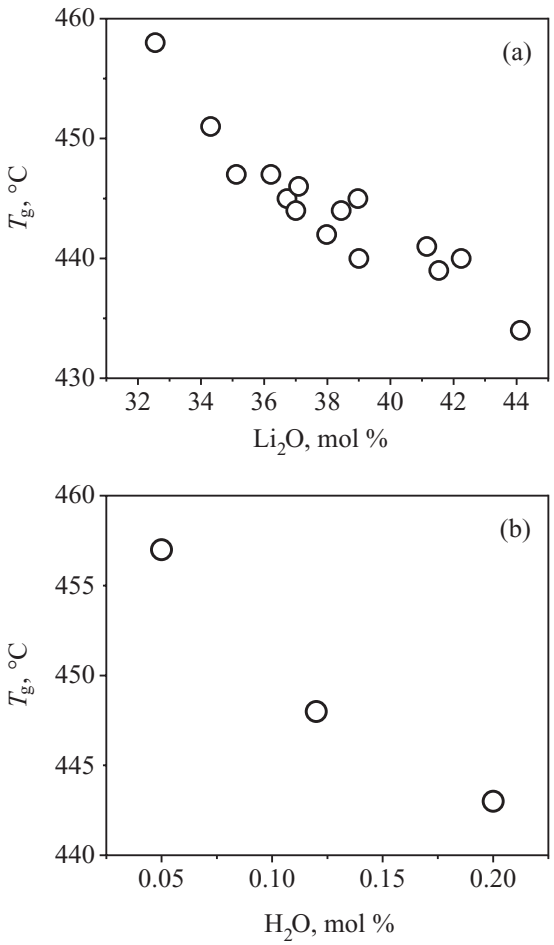

FIG. 2. Glass transition temperatures for lithium silicate glasses versus (a) Li_2O content according to Ref. 21 and (b) water content in LS_2 glass (Ref. 85).

Because viscosity data are often only available for temperatures near and above the melting point T_m (or *liquidus*, T_L) and close to the glass-transition temperature, T_g, due to fast crystallization in the intermediate range, a fitting function $\eta = f(T)$ is needed to interpolate the experimental data between the two extremes. LS_2 glass is just such a case. The most popular equation to fit viscosity data in a wide temperature range is the Vogel-Fulcher-Tammann-Hesse (VFTH) equation:

$$\log \eta = A + \frac{B}{T - T_0}, \tag{1}$$

where η is the viscosity coefficient and A, B, and T_0 are empirical (fitting) parameters. $A \sim -3$ to -4 (Pa s) for oxide glasses, and $0 < T_0 < T_g$ is the temperature where the extrapolated viscosity diverges. At present, there are controversies regarding the physical meaning of T_0 and the VFTH equation, but there is no doubt that it fits viscosity data in the range 10^1–10^{12} Pa s quite well for oxide glasses of widely different fragilities.[70]

Equation (1) can be rewritten in logarithmic form as

$$\eta = \eta_\infty \exp\left(\frac{\Delta G_\eta}{RT}\right), \quad \Delta G_\eta = \frac{2.3BR}{(1 - T_0/T)}, \quad \eta_\infty = 10^A, \tag{2}$$

with a temperature-dependent free activation energy for viscous flow ΔG_η.[71]

The empirical VFTH equation was independently proposed by several authors. Vogel[72] developed it in 1921 based on investigations of the viscosity of some simple liquids, such as water, mercury, and oil, but not of glass-forming liquids. Fulcher[73] used it to analyze the viscosities of several silicate glasses in 1925, and Tammann and Hesse[74] employed it analyzing their results with glass-forming organic substances in 1926. The main success of the VFTH equation stems from the fact that it describes viscosity data over about ten orders of magnitude within 10%. Recently, Mauro *et al.*[75] proposed another description for the viscosity-temperature relationship based on a physically founded model for the configurational entropy (MYEGA equation). According to Mauro *et al.*,[75]

$$\log \eta = A + (12 - A)\frac{T_g}{T}\exp\left[\left(\frac{m}{12 - A} - 1\right)\left(\frac{T_g}{T} - 1\right)\right], \tag{3}$$

where $A = \log \eta_\infty$, m is the fragility parameter, and the glass transition temperature T_g corresponds to a temperature at which the viscosity is 10^{12} Pa s.

It should be noted that all three free parameters (A, m, and T_g) are measurable and have a physical meaning. However, the main value of the MYEGA equation is that it avoids the divergent viscosity at $T_0 > 0$ of the VFTH equation, and also avoids the (unrealistic) divergent configurational entropy in the limit of $T \to \infty$ predicted by the Avramov-Milchev model.[76]

The solid and dotted-dashed lines in Fig. 1 present the results of the fitting procedure of experimental data into

Eqs. (1) and (3), respectively. Both lines with fitting parameters shown in the figure caption are very close to the experimental points, but in our analysis, we will employ Eq. (3).

B. Crystal nucleation

Crystal nucleation occurs via a successful sequence of fluctuations in an melt below the equilibrium melting point and results in the formation of nuclei with critical size R^*. The critical nuclei then advance in the size space via deterministic growth. A measure of the nucleation rate, $I(T)$ [nuclei/m^3 s], is the time frequency of critical nucleus formation per unit volume of melt. Homogeneous nucleation is a process with the same probability of critical nucleus formation in any given volume or surface element of the system under study. According to classical nucleation theory (CNT), the steady-state nucleation rate can be written as (see, e.g., Ref. 71)

$$I_{st} = I_0 \exp\left[-\frac{\Delta G_D + W^*}{k_B T}\right], \quad I_0 = \frac{\sqrt{\gamma k_B T}}{\lambda^2 h}, \tag{4}$$

where k_B and h are the Boltzmann and Planck constants, respectively, and γ is specific surface free energy of the critical nucleus/melt interface. The pre-exponential term, $I_0 \cong N_1 \nu$ (to a first approximation, the number of molecules per unit volume of liquid, N_1, times the characteristic vibration frequency, ν, depends only weakly on temperature) varies between 10^{41} and 10^{43} m^{-3} s^{-1} for different condensed systems.[77] Experimentally measured nucleation rates never reach this limiting value, and the reported maximum for oxide glasses is $\sim 10^{17}$ m^{-3} s^{-1}.[78] The temperature dependence of the nucleation rate is mainly determined by the exponential term, where W^* is the thermodynamic barrier for nucleation, i.e., the increase in the free energy of a system due to the formation of a critical nucleus and ΔG_D is the activation free energy for transfer of a "structural unit" with size λ from the melt to a critical nucleus (the so-called kinetic barrier for nucleation). The latter process is determined by diffusion through a critical nucleus/melt interface. Assuming that this diffusion process is thermally activated

$$D_\tau = \lambda^2 \frac{k_B T}{h} \exp\left(-\frac{\Delta G_D}{k_B T}\right), \tag{5}$$

one can rewrite Eq. (4) as

$$I = \sqrt{\frac{\gamma}{k_B T}} \frac{D_\tau}{\lambda^4} \exp\left[-\frac{W_*}{k_B T}\right]. \tag{6}$$

Time-independent steady-state nucleation is reached when a quasi-stationary size distribution of newly evolving sub-critical ($R < R^*$) and critical ($R = R^*$) nuclei is established in the system. When the quantity of pre-existing nuclei in the parent glass is negligibly small, the following equation for the nucleation time-lag was derived in Ref. 79:

$$\tau_S = \frac{80}{3} \frac{k_B T \gamma}{\Delta G_V^2 \lambda^2 D_\tau}, \tag{7}$$

where ΔG_V is the thermodynamic driving force for crystallization, i.e., the difference between the volume free energies of crystalline and liquid phases per the unit volume of crystal. τ_S corresponds to the time when the nucleation rate practically achieves its steady-state value. The number density N of super-critical nuclei for a given nucleation temperature, T_n, versus nucleation time, t, can be described by the following equation derived by Collins[80] and Kashchiev:[81]

$$N(t) = I_{st} \tau_{C/K} \left(\frac{t}{\tau_{C/K}} - \frac{\pi^2}{6} - 2 \sum_{m=1}^{\infty} \frac{(-1)^m}{m^2} \times \exp\left(-m^2 \frac{t}{\tau_{C/K}}\right)\right). \tag{8}$$

Equation (8) includes two fundamental parameters—the steady-state nucleation rate (I_{st}) and the time-lag for nucleation ($\tau_{C/K}$), which can be estimated as fit parameters. The time scale for the steady-state nucleation, $\tau_{C/K}$, is related to τ_S by $\tau_S \approx 5\tau_{C/K}$. For sufficiently long times compared with $\tau_{C/K}$, Eq. (8) can be approximated by

$$N(t) = I_{st} \left(t - \frac{\pi^2}{6} \tau_{C/K} \right). \tag{9}$$

For the estimation of $\tau_{C/K}$ via Eq. (10), it is sometimes convenient to use the induction period, t_{ind}, which is easily determined as the intersection of the asymptote (Eq. (9)) with the time axis:

$$\tau_{C/K} = \frac{6}{\pi^2} t_{ind}. \tag{10}$$

To estimate the number density $N(t, T_n)$ versus nucleation time at a temperature T_n and then the nucleation rate as $I = dN/dt$, the double-stage method is usually employed. According to this method, used by Gustav Tammann about a hundred years ago[82] and known as the Tammann or the development method,[3,71] the nucleation treatment (T_n, t) is followed by a "development" treatment at $T_d > T_n$ over a sufficiently long time for the nucleated crystals achieve a size that is detectable by microscopy. Because the critical size $R^* = 2\gamma/\Delta G_V$ increases with temperature due to the decrease of the thermodynamic driving force, ΔG_V, only the nuclei that achieved the critical size $R^*(T_d)$ corresponding to the "development" temperature T_d during heat-treatment at T_n can grow at T_d, whereas the nuclei with sizes between $R^*(T_n)$ and $R^*(T_d)$ must dissolve back into the liquid at T_d. Thus, the nuclei need to grow (with rate $U(T_n)$) from $R^*(T_n)$ to $R^*(T_d)$ to survive at T_d. The following relationship between the true kinetic curve $N(t, T_n)$ and the experimental curve $N(t, T_n, T_d)$ estimated by the development method can be written as

$$N(T_n, R^*(T_n), t) = N(T_n, R^*(T_d), t + t_0), \tag{11}$$

where

$$t_0(T_n, T_d) = \int_{R^*(T_n)}^{R^*(T_d)} \frac{dR}{U(T_n, R)}. \tag{12}$$

According to Eq. (12), the higher the growth rate $U(T_n)$ at the nucleation temperature, T_n, and the closer T_d is to T_n (note that $R^*(T_n)$ is correspondingly closer to $R^*(T_d)$), the lower is

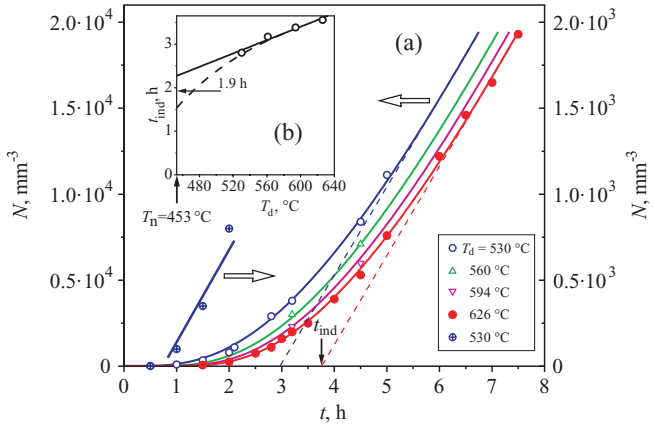

FIG. 3. (a) Number density of $Li_2O \cdot 2SiO_2$ crystals developed at $T_d = 530\,^{\circ}C$ (1, 5), 560 °C (2), 594 °C (3), and 626 °C (4) as a function of nucleation time at $T_n = 453\,^{\circ}C$. (b) Induction time versus development temperature (Ref. 3).

t_0. Hence, the above-discussed effect is expected to be important for low nucleation temperatures and for glasses with a weak overlap of nucleation and growth rate curves. This case holds for LS_2 glass. Fig. 3 shows the $N(t, T_n)$ curves obtained by the "development" method with different development temperatures. The inset shows induction periods $t_{ind}(T_n, T_d)$ versus T_d. Extrapolation of these data to $T_d = T_n$ provides the true value of $t_{ind}(T_n)$ for the given nucleation temperature T_n. The value of $t_0(T_n, T_d)$ can be estimated as

$$t_0(T_n, T_d) = t_{ind}(T_n, T_d) - t_{ind}(T_n). \tag{13}$$

It should be noted that this value of $t_0(T_n, T_d)$ is very similar to that obtained by extrapolating the initial section of the $N(t, T_n, T_d)$ curve (see, e.g., Fig. 3, curve 5) to $N = 0$. Of course, this way of estimating t_0 is easier and less laborious. As expected from Eq. (12) and shown in Fig. 4, the dependence of t_0 on T_n is strong (exponential), similar to $U(T)$, while the dependence on T_d is quite weak, similar to $R^*(T)$.

In connection with the application of the Collins/Kashchiev equation, Eq. (8), a correction, i.e., a shift of the $N(t, T_n, T_d)$ plot by $t_0(T_n, T_d)$ (shown in Figs. 4(a) and 4(b)) is necessary before the fitting procedure because Eq. (8) was derived for nuclei with sizes $R \geq R^*(T_n)$ but not for $R \geq R^*(T_d)$. To illustrate the errors resulting from using the set of non-corrected data, $N(t, T_n, T_d)$ in Eq. (8), we plotted the ideal $N(t)$ dependence via Eq. (8) with $I_{st} = 9.357 \times 10^{11}$ m^{-3} h^{-1} and $\tau_{C/K} = 30.685$ h, then shifted this plot by different periods of time t_0 and fitted into Eq. (8) again. Figs. 5(a) and 5(b) show the fitting results ($\tau_{C/K}$ and I_{st}, respectively) versus t_0. The correction of $\tau_{C/K}(T_n, T_d)$ by $t_0(T_n, T_d)$ does not lead to the true value of the nucleation time-lag (left point corresponding to $t_0 = 0$), and the real values are notably underestimated. This difference is greater for larger values of t_0, according to Fig. 5(a). The incorrect use of the Collins/Kashchiev equation (Eq. (8)) also leads to a slight overestimation of the steady-state nucleation rate, Fig. 5(b). The non-corrected $N(t, T_n, T_d)$ data could be used for analysis with the Collins/Kashchiev equation *only* for low

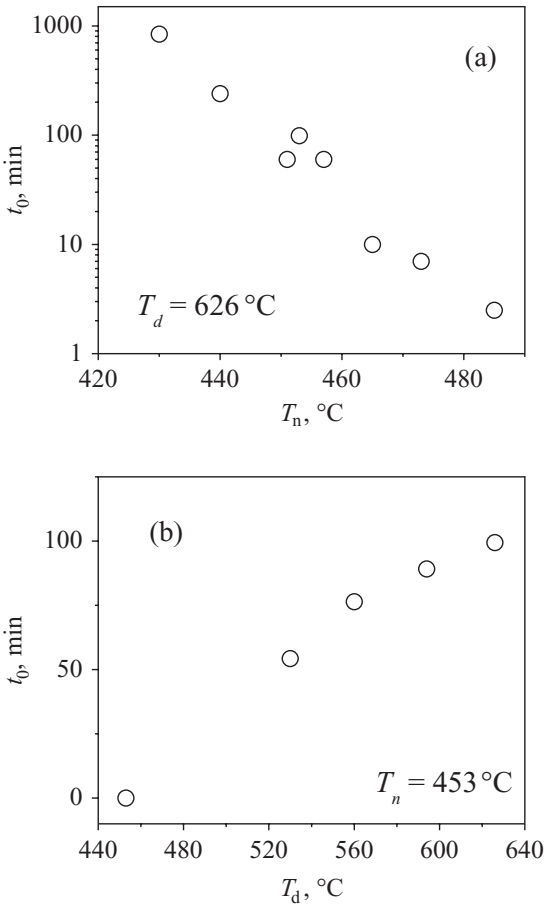

FIG. 4. t_0 versus nucleation temperature, T_n, at given T_d (a) and versus T_d at given T_n (b) for LS_2 glass; data taken from Refs. 8 and 3, respectively.

values of t_0. Thus, according to the above analysis, it is rather desirable to estimate the value of t_0.

1. Effect of composition and water (OH^-) content

As we already mentioned, LS_2 glass has been used for decades as a model glass for the study of multiple aspects of crystallization. Nevertheless, not all authors have published the chemical analysis or estimated the water content of their glasses, although it is known that a deviation from the stoichiometric composition and/or slight differences in trace OH^- concentration leads to notable changes of viscosity and crystallization kinetics, as shown for example in Fig. 2. Thus, Fig. 6 shows the distribution of T_g values reported for lithium disilicate glasses by different authors.[83] The distribution of T_g values taken from papers that often do not include the chemical analysis is quite wide. Taking into account the data presented in Fig. 2(a) (T_g versus Li_2O content), we can assume that the nominal glass composition may differ from the actual composition. However, data from authors who worked with chemically analyzed glasses indicate that the T_g values also show some distribution that cannot be explained by large differences in compositions because the latter does not exceed 0.5 mol.% (Fig. 6, gray columns). Thus, this scatter could reflect the influence of small differences in water concentration, which strongly affects T_g (see Fig. 2(b)). Therefore, as the glasses selected for our analysis have similar viscosity (see

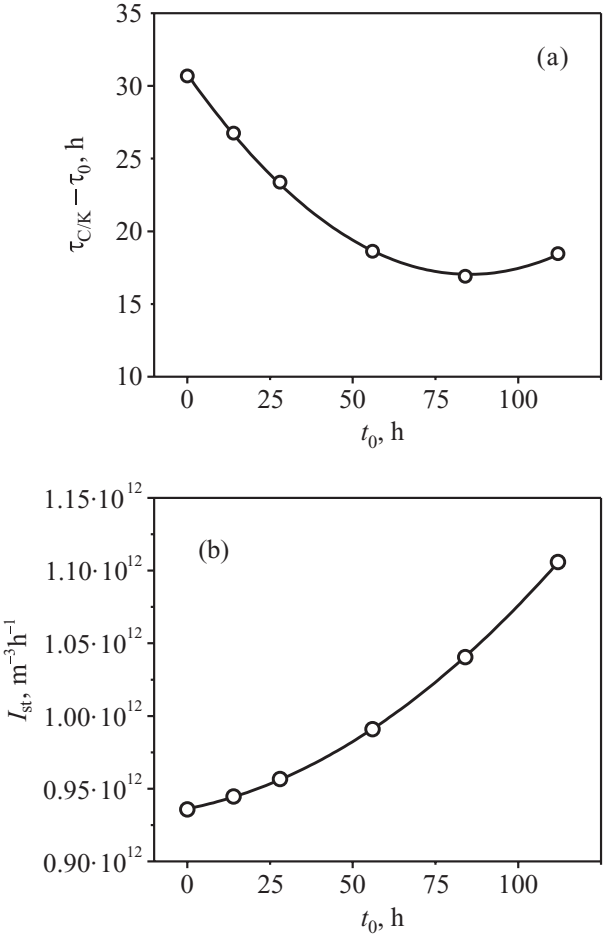

FIG. 5. Dependences of $(\tau_{C/K} - t_0)$ (a) and I_{st} (b) on t_0.

Fig. 1), they should all have similar compositions and water levels. Our fitted viscosity curve may be seen as an average viscosity for LS_2 glass.

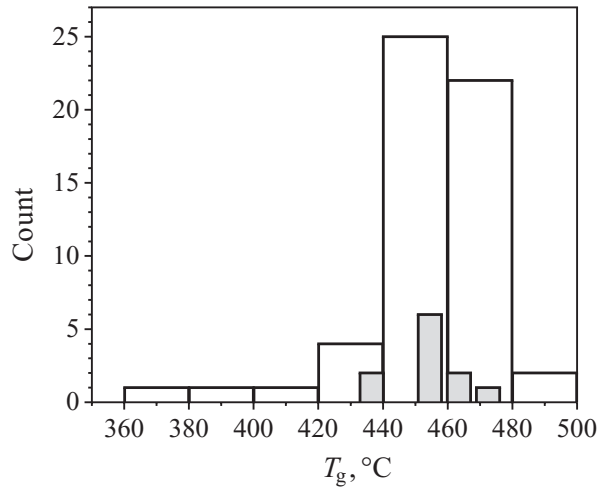

FIG. 6. Distribution of T_g values measured for lithium disilicate glasses by different authors. White and gray bars refer to glasses without and with chemical analysis, respectively. Gray bars refer to glasses for which chemical analysis did not exceed 0.5 mol.% error.

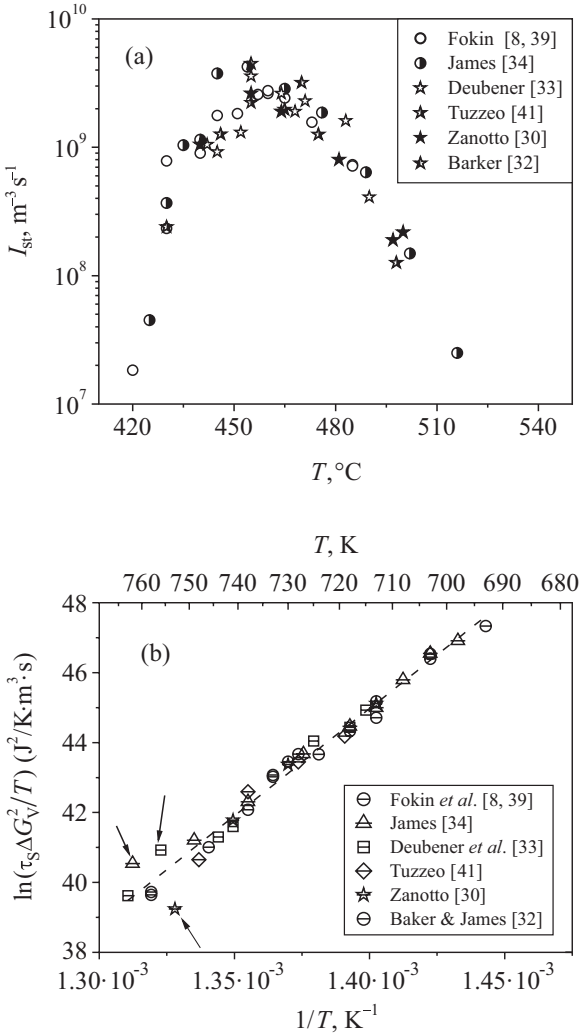

FIG. 7. (a) Steady-state nucleation rates and (b) nucleation time-lags versus temperature and inverse temperature, respectively. The dotted line is the average linear approximation given by $\ln(\tau_s \Delta G_V^2/T) = -40.98 + 61396.39/T$ for all data, excepting the three points marked by arrows.

2. Nucleation rates and time-lags

Steady-state nucleation rates and induction periods or nucleation time-lags were measured in Refs. 4,30–34,37–43 and Refs. 30,32,33,39–41, respectively. Fig. 7(a) shows selected nucleation data from only those papers that provide both I_{st} and t_{ind}. All of these data were obtained by the "development" method with $560 < T_d < 626\,^{\circ}$C, which means that the experimental values of t_{ind} (T_n, T_d) include the true induction period $t_{ind}(T_n)$ together with $t_0(T_n, T_d)$ and thus require correction, which is more pronounced for low nucleation temperatures. Because the development temperatures employed in Refs. 30,32–34,39,41 vary within a relatively narrow interval and the dependence t_0 on T_d is weak (see Fig. 4(b)), we used the values of t_0 shown in Fig. 4(a) to correct the t_{ind} data of the above cited authors. The temperature dependence of τ_S estimated from the corrected value of t_{ind} is presented in Fig. 7(b).

Some comments should be made on the steady-state nucleation rates shown in Fig. 7(a). Out of the almost 100 available data points, only 40% were selected and shown in the

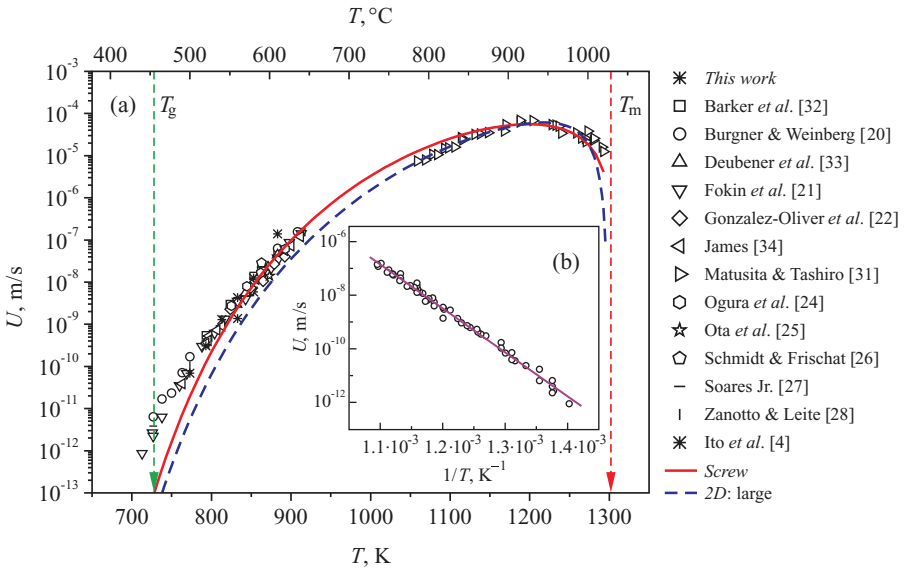

FIG. 8. (a) Crystal growth rates $U(T)$ for $Li_2O \cdot 2SiO_2$ glasses obtained by several authors. (Refs. 20–29 and 32–36) Lines correspond to the screw dislocation SD (solid) and 2D-"large crystal case (dashed line)" growth models with proper fit parameters. SD: fit $\lambda = 0.33$ Å. 2D: fixed jumping distance $\lambda = 4.68$ Å, where $\lambda = (V_M/N_A)^{1/3}$. (b) Inset shows the low temperature data in Arrhenius coordinates, the dashed line is average linear approximation by equation log(U, m/s) = 11.23–16 445.17/T(K).

figure. Despite this selection of nucleation data, some differences are observed between the I_{st} values. There is also a slight trend: the higher is the maximal value of I_{st}, the lower is the temperature of nucleation rate maximum, T_{max}. These facts can be explained by small differences in water content and, therefore, in the kinetic barrier for nucleation because its decrease leads to a shift of T_{max} to lower temperatures accompanied by an increase of I_{st} at T_{max} (see details in Ref. 3).

C. Crystal growth

The crystal growth rates, $U(T)$, are experimentally determined by measuring the crystal size, R, or the thickness of the crystallized layer, h, after various exposure times at certain temperatures in a single-stage treatment. In the existing literature, one finds crystal growth rate data for lithium disilicate glasses between 440 °C and 1020 °C (i.e., from $0.98T_g$ to T_m). These values span eight orders of magnitude, between 10^{-4} and 10^{-12} m/s. Fig. 8 shows selected data on crystal growth rates versus temperature.

Baker *et al.*[32] measured crystal growth rates in an almost stoichiometric glass from 520 °C to 640 °C. They gave indirect indication of the glass composition by considering x-ray (040) peak analysis of crystallized samples and DTA measurements ($T_g = 452$ °C). Burgner and Weinberg[20] prepared a glass with an analyzed composition of (33.3 ± 0.3) Li_2O mol.% and 70 ppm ±10% water and measured internal crystal growth by optical microscopy. Fokin[21,39,84] melted such glass in a platinum crucible and studied the growth rate of $Li_2O \cdot 2SiO_2$ crystals (440–625 °C) along the major axis in the volume of the glass specimens using optical microscopy. James[34] prepared a lithium disilicate glass containing 0.05 wt.% alumina and 0.009 wt.% iron, giving a lithia content of 33.1 mol.%. He measured crystal growth rates from 490 °C to 639 °C using optical and scanning electron microscopy (SEM). Matusita and Tashiro[23] used a glass that deviated from the stoichiometric composition by less than 0.5 wt.% and measured crystal growth rates at 786 °C < T < 1020 °C near the melting point using hot-stage microscopy, reaching a maximum value at 920 °C. The procedure of measuring U was as follows: pieces of glass of 0.02–0.03 g were put into a small Pt crucible and remelted at 1080 °C. The thermocouple was immersed in the melt, removed, and cooled at 900 °C for 5 min still inside the micro-furnace to crystallize the melt adhering on it. Posterior analysis by x-ray diffraction identified the crystals as lithium disilicate. The microfurnace temperature was then lowered to a desired temperature, the thermocouple junction was immersed again in the super-cooled melt, and the crystals growing from the junction into the melt were photographed in 5–10 s intervals. At lower temperatures, the insertion procedure was difficult due to the high viscosity. For this reason, the determination of U was almost impossible at temperatures lower than 750 °C using this technique. Ota *et al.*[25] measured growth rates at 600 °C and 650 °C by optical microscopy and found T_g = 450 °C. Schmidt and Frischat[26] measured crystallization kinetics by SEM and presented chemical analysis by atomic absorption spectroscopy: 33.34 ± 0.03 Li_2O mol.%. Zanotto and Leite[28] observed crystal growth at 500 °C using the heat treatment time from 5 to 95 h. The glass was melted in a Pt crucible and contained 33.2 mol.% Li_2O, 0.02 wt.% of water and 0.01 wt.% Na_2O as the main impurities, in which the levels of Fe and Al were much lower. The crystals were analyzed by optical microscopy only using transmitted and reflected light. Soares, Jr.[27] studied crystal growth at T_g (454 °C) by TEM and also performed chemical analysis, with results close to stoichiometric composition. Gonzalez-Oliver *et al.*[22] produced five glasses, but the authors chose the L1 glass (33.1 Li_2O mol.%) because of its minor water content

(0.02 OH wt.%) and presented results of chemical analysis (flame photometry). They measured the thickness of the thin surface crystallization layer as a function of time using polished sections, observing that U was constant with time at each temperature. X-ray analysis of crystallized samples confirmed that the crystalline phase was LS_2. The composition determined from chemical analysis by Deubener *et al.*[33] was (33.5 ± 0.4) $Li_2O \cdot$ (66. 5 ±0.4) SiO_2, and optical and TEM techniques were employed. Ogura's *et al.*[24] glass was close to the stoichiometric composition, and as done as by Degen and Toropov,[29] they measured the thickness of a crystallized surface layer by the quenching method using optical microscope. Ito *et al.*[4] studied the rate of crystal growth for surface and internal crystallization, but we considered in this work only results for the long axis of internal crystals, between 500 °C and 610 °C. Leontjeva used the quenching method, and three of seven measurements were approximated.[35] Parcell[36] used an indirect method and determined growth from the crystallized layer by thermoanalytical process. Some results on growth kinetics are far above the data set presented by others, specifically the works of Degen and Toropov,[29] Leontjeva,[35] and Parcell.[36] However, not all authors performed chemical analyses of studied glass, although it is known that it diverges from stoichiometry and impurity levels. In particularly, water can affect the growth rate (see, e.g., Ref. 85 how water content affects LS_2 glass). As an extreme example, in "pure" SiO_2 glasses, U varies by more than an order of magnitude with a few ppm alkali impurities or "water".[79,80] Therefore, in the forthcoming analysis, we do not employ marginal data such as those from Refs. 29, 35 and 36. They were discarded to guarantee the closeness of the used compositions to lithium disilicate. However, the results from 13 of 17 available papers, corresponding to about 100 measurements, presented in Fig. 8 agree quite well in a temperature range of 600 °C and are thus be used in this paper.

Here, it is important to note that the crystal morphology in LS_2 glasses varies from an ellipsoid of revolution with growth rates U_{min} and U_{max} along the minor and major diameters, respectively, (see, e.g., Ref. 84) at low temperatures, to a spherulitic form at high temperatures.[23] All data collected in Fig. 8 refer to U_{max}.

1. Growth models

Three phenomenological models are frequently used to describe crystal growth kinetics controlled by molecular rearrangement at the crystal-liquid interface: normal growth, screw-dislocation-mediated growth and that by two-dimensional (2D) secondary surface nucleation.[71,86–92] According to Jackson's treatment of the interface,[71,88,89] materials with high melting entropy (>4R), such as lithium disilicate ($\Delta S_m = \Delta H_m/T_m \cong 4.9R$, where ΔH_m is the melting enthalpy, 57.3 kJ/mol), are expected to exhibit crystal growth kinetics of the form predicted by either the screw dislocation or the 2D surface nucleation growth models.

These two models will be tested in the next paragraphs. To a first approximation for both analyses, we will estimate the effective diffusion coefficient D_U (which is responsible for the mobility of elements on the crystal/melt interface) via the SEE equation, which connects the (volume) shear viscosity coefficient, η, with the volume effective diffusion coefficient, D^{η}_{eff}:

$$D^{\eta}_{eff} \cong \frac{k_B T}{\lambda \eta}, \tag{14}$$

where λ is the diameter of the diffusing molecules or the jump distance.

In the case of crystal growth in its own melt, the value of D_U could differ from D^{η}_{eff} because D_U relates to processes on the crystal/melt interface, while D^{η}_{eff} refers to diffusion within the melt interior. Thus, we neglected this fact in these preliminary analyses, but we will return to this problem in Sec. III.

a. Screw dislocation. According to the *screw-dislocation* growth model, the crystal-liquid interface is smooth but imperfect on an atomic scale and growth takes place at step sites provided by screw dislocations intersecting it. The corresponding temperature dependent growth rate U may be expressed by

$$U = f \frac{D_U}{\lambda} \left[1 - \exp\left(-\frac{\Delta G}{RT} \right) \right], \tag{15}$$

where D_U is an effective diffusion coefficient that controls atomic or molecular attachment at the interface; λ is the diameter of the diffusing building molecules; ΔG is the free energy change upon crystallization (J/mol), as introduced in Eq. (7), the thermodynamic driving force for crystallization; R is the gas constant; and f is the fraction of preferred growth sites at the interface (i.e., dislocation edges). λ is equivalent to the jump distance, the lattice parameter, or the unit distance advanced by the interface, which are usually taken in such kinetic analyses. The value of f is given by[71,88–92]

$$f = \frac{\lambda \Delta G}{4\pi \gamma V_M}, \tag{16}$$

where V_M is the molar volume of the crystal.

For small undercoolings, $\Delta T = (T_m - T)$, f follows the form $f = \Delta T / 2\pi T_m$ derived with the use of the semi empirical equation proposed by Skapski and Turnbull[93,94] for the surface energy γ.

In the case of *normal* growth ($\Delta S < 2R$), Eq. (15) still applies with $f \sim 1$. One normally uses the limiting values of $\Delta G \equiv \Delta G_V V_M$ calculated by the Thomson ($\Delta G = \Delta H_m \Delta T / T_m$) or Hoffman ($\Delta G = \Delta H_m T \Delta T / T_m^2$) approximations,[71,88,89,95] where ΔH_m is the melting enthalpy per mol. Here, we were fortunate enough to have experimental data for ΔG (see Eq. (17)) from Ref. 96. However, the results of the kinetic analysis from Eq. (15) obtained using these two approximations and those with Eq. (17) presented almost identical results because, according to Eq. (15), the crystal growth rate depends on ΔG weakly as compared with D_U. The thermodynamic driving force experimentally measured in Ref. 96 for LS_2 can by approximated in the temperature range of our interest by the following polynomial, with

ΔG in J/mol and T in K:

$$\Delta G = 53399 - 42.015T + 0.00713T^2 - 4.79 \times 10^{-6}T^3. \quad (17)$$

By employing Eqs. (14) and (16), Eq. (15) can be rewritten in the following form:

$$U = \frac{1}{\lambda}\frac{\Delta G}{\eta}\frac{k_B T}{4\pi\gamma V_M}\left[1 - \exp\left(-\frac{\Delta G}{RT}\right)\right], \quad (18)$$

which we will use to fit the experimental data, $U(T)$, using λ as the only fitting parameter.

b. Surface nucleated growth (2D) model. In the *2D secondary nucleation* growth model, the surface of the primary crystals is considered atomically smooth and free of defects. Growth takes place by the formation of two-dimensional nuclei on the top of the primary crystals. The growth rate is expressed by[20,71,88–90,92]

$$U = C\frac{D_U}{\lambda^2}\exp\left(-\frac{Z}{T\Delta G}\right). \quad (19)$$

Substituting D_U by D_{eff}^{η} (as was done in the above paragraph), we can rewrite Eq. (19) as

$$U = C\frac{k_B T}{\lambda^3\eta}\exp\left(-\frac{Z}{T\Delta G}\right). \quad (20)$$

Parameters Z and C in the above equations are different for the cases of *small* and *large* crystals:

$$Z = \frac{\pi\lambda V_m\gamma^2}{k_B} \quad \text{(small crystal)}, \quad (21)$$

$$Z = \frac{\pi\lambda V_m\gamma^2}{3k_B} \quad \text{(large crystal)}, \quad (22)$$

where γ is the surface edge energy of the 2D crystal for growth, usually taken as the liquid-crystal surface energy cited above.

$$C = \lambda N_S A_0 \quad \text{(small crystal)}, \quad (23)$$

$$C = \frac{\sqrt[3]{(\pi/3)N_S\lambda^5}}{\Gamma(4/3)}\left[1 - \exp\left(-\frac{\Delta G}{RT}\right)\right]^{2/3}, \quad \text{(large crystal)}, \quad (24)$$

where A_0 is the cross-sectional area of interface, $N_S \sim 1/\lambda^2$ is the number of molecules (formula units) per unit area of interface, and Γ is the gamma function.[20,71,88–90,92] The notations *small* and *large* are relative to the following: (a) The *small* crystal case refers to when the secondary nuclei grow across the interface in times that are short compared with the time between nucleation events. (b) The opposite situation is denoted as a *large* crystal case.[88–90,92] The *large* crystal case is applied for a general situation.

To describe the experimental $U(T)$ data, we employed two models (screw dislocation and surface nucleated growth—large crystal type) using the fitted viscosity data via the MYEGA equation.[75] The solid and dotted lines in Fig. 8 were calculated by Eqs. (18) and (20), respectively. For the case of the screw dislocation growth model (solid line), we employed the jump distance as the fit parameter ($\lambda = 0.33$ Å) and fixed $\gamma = 0.15$ J/m^2 (or ~0.18 J/m^2 if a temperature independent gamma is fitted to the nucleation rate data) from the nucleation rate analysis[3,89] for the same glass. For the analysis with the 2D secondary surface nucleated growth model (dotted line), we used γ as a fit parameter ($\gamma = 0.048$ J/m^2) with a pre-fixed size parameter $\lambda = \sqrt[3]{V_M/N_A} = 4.68$ Å.

Analysis of Fig. 8 shows the best fits using the *screw dislocation* and *2D surface nucleation* growth models. Both curves are rather close to the experimental data. It should be emphasized that, strictly speaking, a fitting procedure is not the best way to ascertain the true model. Indeed, an analysis of the temperature dependencies of the reduced crystal growth rate U_R at low undercoolings,

$$U_R = \frac{U\eta}{1 - \exp(-\Delta G/RT)}, \quad (25)$$

performed by the method proposed by Uhlmann *et al.*[89] shows that the *screw dislocation* model is most likely for LS_2. Therefore, we will use this model in the forthcoming analysis.

D. Ionic conductivity

For glass-forming systems in the solid or super-cooled liquid state, ionic transport due to alkali cations strongly depends on temperature. The variations of the conductivity-temperature product σT in an Arrhenius representation show two distinct behaviors. At the lowest temperatures, the product follows an Arrhenius relationship:

$$\sigma T = A_\sigma \exp\left(-\frac{E_A^\sigma}{RT}\right), \quad (26)$$

where A_σ and E_A^σ are constants. In this temperature range, for all ionic conducting glasses, the representation of experimental data of $\log_{10}(\sigma T)$ depending on $1/T$ results in straight lines (as shown in Fig. 9) that converge to $\log_{10}A_\sigma$ at infinite temperatures. This Arrhenius behavior can be described by a classical approach initially developed for ionic crystals and then extended to ionic conductive glasses (see, e.g., Ref. 97 as a recent reference on subject).

At higher temperatures, above T_g, another mechanism is observed in addition to the low-temperature hopping process: local deformations of the silicate chains enable the transfer of Li^+ to other positions and may be associated with a free volume mechanism.[97] The experimental data obey an empirical rule proposed by Dienes[98] and later by Macedo and Litovitz,[99] which was originally established to describe the viscosity-temperature dependence of molten silicates:

$$\sigma T = A_\sigma^* \exp\left(-\frac{E_A^*}{RT}\right)\exp\left[-\frac{B_\sigma}{R(T - T_0)}\right], \quad (27)$$

where A_σ^*, B_σ, T_0, and E_A^* ($E_A^* < E_A^\sigma$) are constants. It should be noted that the apparent "activation enthalpy" for conduction at high temperatures depends on temperature.

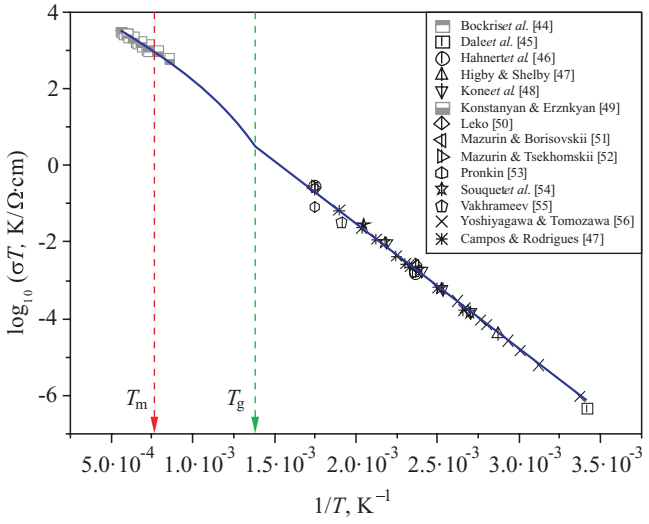

FIG. 9. Temperature dependence of ionic conductivity in LS_2 glass.

Experimental data near T_m and an application of Eq. (27) are shown in Fig. 9. Refer to Refs. 100 and 101 for more details on the theory expressed by Eqs. (26) and (27) and the obtained values.

III. DISCUSSION

The plethora of dynamic property data presented above is connected to diffusion processes and, thus, provides a unique opportunity for performing an extensive comparative analysis and estimating the effective diffusion coefficients that control viscous flow and crystallization. To boost such an analysis, we employed additional data on the self-diffusion coefficients of ionic species Si^{4+}, O^{2-}, and Li^{+} estimated from real experiments and kindly calculated using MD simulations by Gonçalves and Rino[102] at our request.

Fig. 10 summarizes all of the different diffusivities measured or calculated in a wide temperature range from above the melting point to below the glass transition range. It is important to note that it includes viscous flow and crystal growth measurements from different authors in a wide temperature interval. To the best of our knowledge, this work is one of the most complete set of diffusion processes ever collected, calculated, and analyzed for an oxide glass-forming system. It covers six different transport processes spanning 16 orders of magnitude in a wide range of temperatures from above T_m to below T_g!

The high temperature interval in Fig. 10 shows the following:

i. D^{σ}_{Li}: estimated from conductivity data[44,49] by the Nernst-Einstein equation (the subscript Li is used because Li^{+} is responsible for the charge transport in LS_2 glass),

$$D^{\sigma}_{Li} = \frac{\sigma k_B T}{N_{Li} e^2}, \tag{28}$$

where e is the electronic charge and N_{Li} is the concentration of Li^{+} ions (number of ions/m^3). For lithium disilicate, we estimated N_{Li} as 5×10^{28} m^{-3} from density data ($d = 2.34$ g/cm^3) considered, to a good approximation for this partial goal, a constant from below T_g up to far above T_m.

ii. $D_{Li\text{-}Si}$: measured Li-Si inter-diffusion by Kawakami *et al.*[61] It is reasonable to consider this coefficient approximately equal to the silicon diffusivity, D_{Si}, because the slowest species determines inter diffusion. This assumption was confirmed by MD simulations (see below).

iii. D^{MD}_{Si}, D^{MD}_{O}, and D^{MD}_{Li} independently estimated by MD simulations.[102]

The temperature interval below T_g shows the following:

i. D_{Li}: self-diffusion coefficients measured by Beier and Frischat[58] and D^{σ}_{Li} estimated from the conductivity data of Refs. 51–55 and 57 considering Eq. (28).

ii. D^{O}: measured self-diffusion coefficients of oxygen reported by Sakai *et al.*[59] and Takizawa *et al.*[60]

iii. D_{τ}: calculated here from experimental nucleation time-lags.

Fig. 10 shows that, somewhat surprisingly, the results of MD simulations are in excellent agreement with the respective ionic diffusivity determined in real experiments: $D^{MD}_{Li} \cong D^{\sigma}_{Li}, D^{MD}_{Si} \cong D_{Li-Si}$!

The values of D^{MD}_{O} at high temperatures are very close to D^{MD}_{Si} (and to the interdiffusion data D_{Li-Si}). It should be emphasized that all above diffusivities relate to processes occurring within the melt *volume*. The effective (overall) volume diffusivity D^{V}_{eff} can be calculated from the diffusivity of the individual elements and the melt composition by[90,103]

$$D^{V}_{eff} = \frac{1}{\frac{x_{Li}}{D_{Li}} + \frac{x_{O}}{D_{O}} + \frac{x_{Si}}{D_{Si}}}, \tag{29}$$

where x_i denotes the molar/atomic fraction of the i-components in the melt.

The dashed line in Fig. 10 shows the D^{V}_{eff} calculated by Eq. (29). As expected, this quantity is controlled by the slowest species and the line is located very close to D_{Si} and D^{MD}_{O} (the slowest species). It should be noted that this same effective diffusion coefficient appears in the SEE Eq. (14) considering $\lambda = 2.7$ Å.

Fig. 10 also shows the effective diffusion coefficients estimated from the nucleation time-lags (D_{τ}) via Eq. (7) and crystal growth rates (D_U) with Eq. (30), which results from a combination of Eqs. (15) and (16):

$$U = D_U \frac{\Delta G}{4\pi\gamma V_M}\left[1 - \exp\left(-\frac{\Delta G}{RT}\right)\right]. \tag{30}$$

As opposed to Eq. (7), Eq. (30) does not include the (unknown) size parameter, λ. For calculations with Eq. (30), we used $\gamma = 0.15$ J/m^2.[3,91] When estimating D_{τ} via Eq. (7), we employed the same value of γ and $\lambda = 2.7$ Å.

Because the effective diffusivity D^{η}_{eff} in the SEE Eq. (14) and the effective diffusion coefficients estimated via Eq. (29) refer to volume diffusion, $D^{\eta}_{eff} \approx D^{V}_{eff}$. To fulfill this condition, the jump distance, λ_{η}, in the SEE Eq. (14) was used as an adjustable parameter. This procedure led to $\lambda_{\eta} = 2.7$ Å, which is comparable to the Si−O bond length (1.9 Å), the LS_2 molecule size $\lambda = (V_m/N_A)^{1/3} = 4.7$ Å, and λ_{MD}

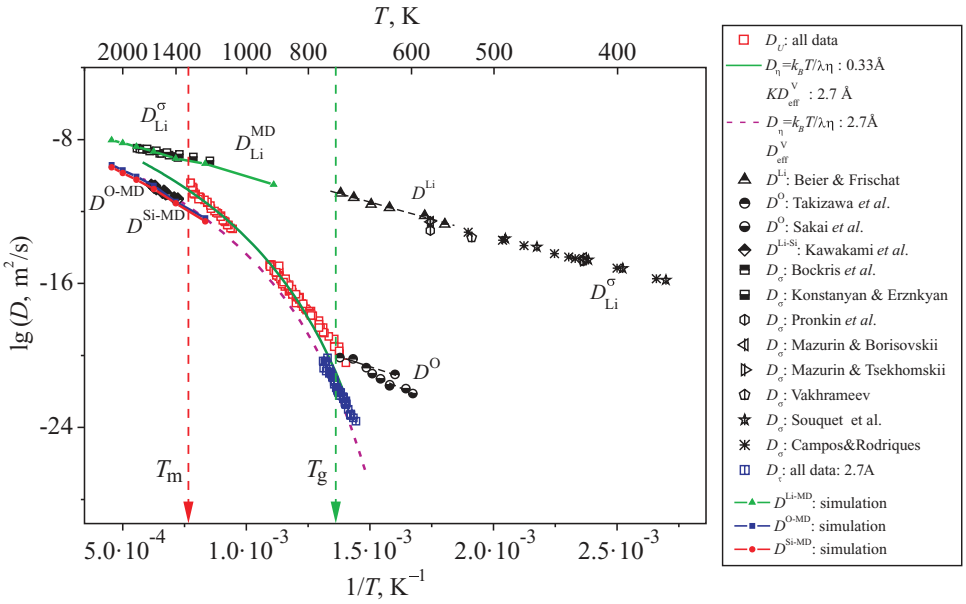

FIG. 10. Measured and calculated diffusion coefficients in LS_2 liquid from above the melting point to below T_g for different transport processes: crystal growth, viscous flow, nucleation time-lag, conductivity, self-diffusion, and MD simulations. Check the list of symbols on the right side of the figure and the text for more detailed explanations.

= 2–4 Å estimated by equating the SEE equation for the experimental viscosity data and the Si diffusion coefficient. This fact emphasizes that the viscosity curve of a perfectly pure and stoichiometric LS_2 glass (such as that created in the MD simulations) would likely be larger than that of a real glass (which has water and impurities) and, thus, the following inequality $\lambda_{MD} < \lambda_\eta$ is expected. Thus, λ_η is about 8 times larger than $\lambda_U = 0.334$ Å, previously estimated as the fit parameter (see Sec. II C) to the experimental crystal growth rates via Eq. (18), which corresponds to the screw dislocation growth model. One should recall that in this analysis, we substituted the effective diffusion coefficient, D_U, with the effective viscosity coefficient via the SEE equation assuming that $D_U = D^\eta_{eff}$. By proceeding in such a way, we supposed that the effective volume diffusivity (D^η_{eff}) controls the growth process. Perhaps this assumption could be true in highly nonstoichiometric crystallization, when the crystal composition is far from the melt composition and "long-range" transport of the building elements through a diffusion zone is needed. However, because the composition of the (measured) micron-sized crystals in our case is the same as that of the liquid, the growth process is mainly determined by the mobility of the species that are *on* and *near* the crystal/melt *interface* and not within the overall melt volume. As we already noted, this process is similar to diffusion through an interface or short-range structural rearrangement. Therefore, the validity of the assumption $D_U = D^\eta_{eff}$ is questionable, and it is thus reasonable to assume that $D_U > D^\eta_{eff}$ and $D_U = K D^V_\eta$ with $K > 1$. This new assumption allows us to describe $U(T)$ with $D_U > D^\eta_{eff}$ and the jump distance $\lambda_\eta = 2.7$ Å, which was obtained above from the condition $D^\eta_{eff} = D^V_{eff}$. In this case, Eq. (18) can be rewritten as

$$U = \frac{K}{\lambda_\eta}\frac{\Delta G}{\eta}\frac{k_B T}{4\pi\gamma V_M}\left[1 - \exp\left(-\frac{\Delta G}{RT}\right)\right], \tag{31}$$

where

$$K = \frac{\lambda_\eta}{\lambda_U}. \tag{32}$$

By setting $\lambda_\eta = 2.7$ Å and $\lambda_U = 0.334$ Å in Eq. (32), we obtain $K \cong 8$. This value indicates that the diffusivity *near* and *on* the crystal/liquid interface determining crystal growth could be eight times faster than that in the melt volume in the case of LS_2. It should be noted that such acceleration does not need a significant decrease in the activation free energy of the process. Thus, we arrived at a self-consistent description of the three independent groups of experimental data: viscosity, effective diffusion coefficients in the melt, and crystal growth. With the same value of λ, we satisfied the condition $D^\eta_{eff} \approx D^V_{eff}$ and described the experimental dependence $U(T)$ employing $D^U_{eff} = K D^V_{eff}$. Moreover, we could estimate the value of K. It should be also noted that the calculation of U with new parameters (λ_η and $D^U_{eff} = 8 D^\eta_{eff}$) results in the same curve $U(T)$ that is shown in Fig. 8.

Returning to the data of Fig. 10, one can see that at high temperatures the $K D^\eta_{eff}(T)$ curve (dark green, full line) estimated from viscosity by the SEE equation with $\lambda_\eta = 2.7$ Å matches the values of D_U, which were independently calculated from the crystal growth rates via Eq. (30). However, at low temperatures, beginning at $T \equiv T^U_d \approx (1.10 - 1.13)T_g$, a breakdown of the Stokes-Einstein/Eyring equation occurs; the viscosity increases with decreasing temperature faster than the effective diffusion coefficient D_U decreases. Hereafter, we will refer to T_d as the decoupling temperature because there is a decoupling between the transport processes controlling crystallization and viscous flow. To demonstrate this fact more clearly, we plotted the D_U/D^η_{eff} ratio versus temperature in Fig. 11.

According to Fig. 11, at temperatures above T^U_d, the effective diffusion coefficient at the crystal/melt interface is

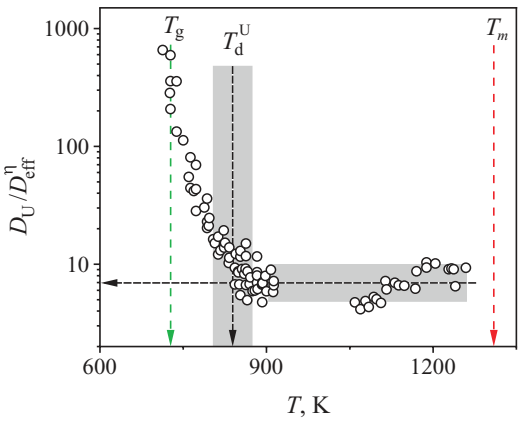

FIG. 11. Ratio of diffusion coefficients controlling crystal growth D_U and viscous flow D_{eff}^{η} as a function of temperature showing decoupling at $\sim 1.1T_g$.

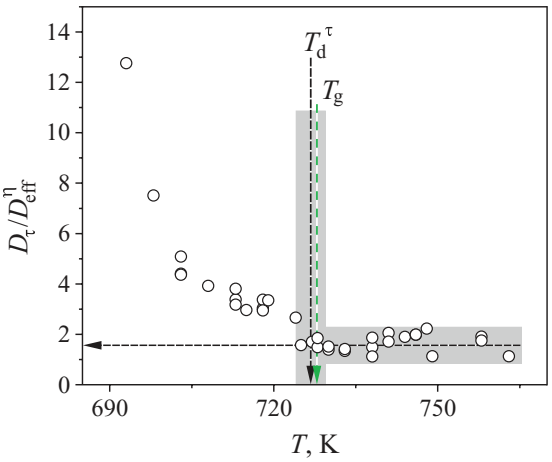

FIG. 12. Ratio of diffusion coefficients controlling nucleation time-lags D_{τ} and D_{eff}^{η} as a function of temperature showing decoupling at $\sim T_g$.

higher than that connecting (volumetric) viscous flow by a factor of about 8; see also Fig. 10. For completeness, however, the reader should be informed that for at least two silicate systems, diopside[90] and silica,[86,87] the ratio D_U/D_{eff}^{η} is close to unity. We will dwell more on this particular issue in a future publication devoted exclusively to analyzing this ratio in several silicate liquids,[104] but we can advance that, except for silica and diopside, differences from 5 to 10 times are also observed for other silicates. In addition, beginning at the decoupling temperature, T_d^U, this difference starts to increase drastically with decreasing temperature, giving strong evidence for the breakdown of the SEE equation.

The notable difference in the values of the effective diffusion coefficients for crystal growth and nucleation processes and their activation enthalpies (see Fig. 10) corroborates the results presented and discussed in Ref. 91. These experimental facts were interpreted in Ref. 91 as a strong support that even for the so-called polymorphic crystallization, the nucleating phase may have a different composition and/or structure compared to the parent glass and the newly evolving macro-phase. Considering the comparative analysis of the diffusion coefficients governing viscous flow and crystallization kinetics as the main problem addressed in this paper, we employed the same thermodynamic driving force for macro-crystals (growth) and critical nuclei (time-lag for nucleation). We neglected the possible decrease in the values of ΔG for nucleation for the following reasons: first, the reducing factor for ΔG is not known and second, this correction will not change, at least qualitatively, the main results of the present analysis.

A. Nucleation

The data on D_{τ} and D_{eff}^{η} are shown in Fig. 12 in a form similar to Fig. 11. Fig. 12 also demonstrates decoupling between the effective diffusion coefficient D_{τ} responsible for the formation of critical nuclei and the diffusion coefficient D_{eff}^{η} of the SEE equation. However, in contrast to T_d^U, T_d^{τ} is very close to the glass transition temperature, T_g. This fact is very important for the analysis of the effect of elastic stresses (which arise due to the difference in the melt and crystal densities) on nucleation rates because *nucleation* is responsible for stress production whereas *viscous flow* leads to stress relaxation. The decoupling of these two processes at about T_g (where the homogeneous nucleation rate maximum is generally located) corroborates the recent theoretical and experimental studies on the role of elastic stresses in glass crystallization (see Appendix A). Moreover, it indicates that viscosity can indeed be used above T_g to analyze nucleation rates. However, this conclusion requires more data on the time-lags extending to the high temperature range ($T \gg T_g$). Unfortunately, this aim has a serious hurdle to overcome: the extremely low values of time-lag for nucleation in this temperature range.

The other distinctive feature of the data shown in Fig. 12 is that above the respective decoupling temperatures, D_{τ} differs from D_{eff}^{η} by only a factor of 2 or less, whereas D_U exceeds D_{eff}^{η} by about 8 times (compare Figs. 11 and 12). This distinction may reflect a difference in the mechanisms that commands the advance in the size space: fluctuations for sub-critical nuclei and deterministic growth for super-critical crystals, which is determined by the mobility of "building" units on and near a well defined crystal/melt interface. The evolution of the interface properties with nuclei size should be also taken into account; it is reasonable to assume a diffusive interface in the case of sub-critical nuclei and a well-formed boundary for macro-crystals. The last case allows one to suppose the faster incorporation of "building" units on the boundary of the critical nuclei as opposed to the diffusion boundary of the critical nuclei.

B. Possible explanation for the breakdown of the SEE equation

It has been experimentally established that the Stokes-Einstein/Eyring relationship holds for equilibrium silicate liquids over a wide temperature range (see, e.g., Ref. 92), and well below T_m for very strong liquids.[86,87] Its validity at $T_d < T < T_m$ indicates that the transport processes that control crystallization and viscous flow are equal or very similar and include the same structural species. Indeed, as shown above,

the effective diffusion coefficient D^{η}_{eff} estimated from the SEE equation varies with temperature above the decoupling temperature, T^{U}_{d}, in the same way as the effective diffusion coefficients independently estimated from the individual self-diffusion coefficients of Si^{4+}, O^{2-}, and Li^{+} or from experimental crystal growth rates. However, as the glass transition temperature is approached from above, the SEE equation fails and thus can no longer be employed to describe the temperature dependence of crystal growth, which is determined by the mobility of the "building" units.

The breakdown of the SEE equation at $T_d \geq T_g$ verified for deeply undercooled fragile organic and metallic liquids has been reasonably ascribed to spatially *dynamic heterogeneity* (e.g., Refs. 105 and 106). This phenomenon is due to a wide distribution of "molecular" groupings within the undercooled liquid with widely different relaxation times. According to several authors, e.g., Ref. 107, the decoupling phenomenon are explained by the characteristic time scale for a highly cooperative process, such as viscous flow, is governed by the *slower* contributions to the distribution of structural relaxation times, $D_{\eta} \sim \langle \tau_s \rangle^{-1}$, whereas below T_d, the average relaxation times for crystal growth are governed by the *faster* contributions: $D_U \sim \langle \tau_s{}^{-1} \rangle$. For a liquid with a very narrow distribution of relaxations times, such as above T_m, or a very strong glass-forming liquid such as silica, the following holds: $\langle \tau \rangle^{-1} \sim \langle \tau^{-1} \rangle$. Below T_m, the distribution of relaxation times becomes wider with decreasing temperature, a tendency that is more pronounced for fragile liquids that show stronger dynamic heterogeneity, e.g., Ref. 107, such as LS_2 glass.

To corroborate the concept of different structural groups controlling structural rearrangements, NMR experiments and thermodynamic modeling clearly indicate that significant fractions of Q^2 (2Li-2NBO-Si-2BO-2Si-) = 25%; Q^3 (1Li-1NBO-Si-2BO-2Si-) = 50%; and Q^4 (-2Si-2BO-Si-2BO-2Si-) = 25% molecular groups co-exist at T_g in this glass.[108] These different molecular groups can give rise to *dynamic heterogeneity* and decoupling.

IV. CONCLUSIONS

i. At high temperatures near T_m, the temperature dependences of the effective volume diffusion coefficients D^{V}_{eff} (estimated via the ionic diffusivities of Li^{+}, Si^{4+}, and O^{2-}) and the effective diffusion coefficients D^{η}_{eff} (estimated by the SEE equation) are similar and their values agree for a reasonable value of jump distance, $\lambda = 2.7$ Å. These facts confirm the validity of the SEE equation in the high-temperature range.

ii. In a wide temperature range from T_m down to $T^{U}_{d} \sim 1.1T_g$, the crystal growth rates are well described by the screw-dislocation model. The *temperature dependence* of the effective diffusion coefficient that controls crystal growth, D^{U}_{eff}, agrees with D^{η}_{eff} calculated from the viscosity. This fact corroborates the consistency of the SEE equation at high temperatures, for viscosities below $\sim 10^7$ Pa s. However, to employ viscosity data for the calculation of crystal growth rates, one has to take into account that D^{U}_{eff} is about 8 times higher than D^{η}_{eff}. This difference may reflect the faster diffusivities of the building units that are on or near the crystal/melt interface.

iii. Beginning at the decoupling temperature, T^{U}_{d}, the ratio $D^{U}_{eff}/D^{\eta}_{eff}$ drastically increases with decreasing temperature, indicating a clear breakdown of the SEE equation for $T < T^{U}_{d}$. Therefore, one cannot use viscosity data to estimate crystal growth rates in this temperature range.

iv. Similar decoupling occurs between D^{η}_{eff} and the effective diffusion coefficient, D^{τ}_{eff}, estimated from the nucleation time-lags, but at lower temperature $T^{\tau}_{d} \sim T_g < T^{U}_{d}$. Hereby, at temperatures higher than T_g, the diffusion coefficient D^{τ}_{eff} is closer to D^{η}_{eff} and exceeds the latter by only a factor of 2. The above differences in $D^{\tau}_{eff}(T)$ and $D^{U}_{eff}(T)$ indicate a distinction in the types of interfaces and mechanisms of critical nuclei formation (nano-crystals) and growth of macro-crystals.

v. The possible precipitation of metastable phases in the early stages of crystallization, internal stresses caused by crystallization, and a change of crystal morphology cannot be responsible for the observed decoupling between viscous flow and crystallization.

Based on well-established knowledge, one can reasonably speculate that below the decoupling temperature, the diffusion process must be commanded by spatially *dynamic heterogeneity*. The characteristic time scale for viscous flow (a highly cooperative process) is governed by some large groupings of atoms possibly involving several "molecules" (such as -Si-BO-Si-BO-) that have the slowest contributions to the distribution of structural relaxation times, whereas the average times for crystallization is governed by the faster molecular groups (-Si-NBO-Li^{+}).

To shed light into the transport mechanism, we compared the three calculated diffusivities with the diffusion coefficients of Li^{+}, O^{2-}, and Si^{4+} measured in real experiments and from MD simulations. At low undercoolings near T_m, an effective diffusion coefficient D^{V}_{eff}, calculated by a combination of diffusion coefficients for Si, O, and Li within a hypothetical $Li_2Si_2O_5$ "molecule", describes the temperature dependence of viscosity and crystal growth rates with the same reasonable jump distance, $\lambda \approx 2.70$ Å. However, at deep undercoolings *below* T_d, Li^{+} ions diffuse several orders of magnitude too fast, and even D_O is much faster than D_U, D_{τ}, and D_{η}. Unfortunately, no data are available for D_{Si}.

Taken *in toto,* the results of the present study give significant insights on the diffusing species controlling flow and crystallization in this important glass-forming liquid. It also validates the use of viscosity to account for the transport term of the crystal growth equation for temperatures above, but not below, $T_d \sim 1.1T_g$. The same rule applies to nucleation time-lags, but in this case, $T_d \sim T_g$. Therefore, a very important implication is that one can use viscosity data to analyze nucleation kinetics above T_g.

ACKNOWLEDGMENTS

Financial support from Brazilian funding agencies CAPES, CNPq and FAPESP in the form of Grant

No. 04/10703-0, 305373/2009-9, 479799/2010-5, and 07/08179-9 are fully appreciated. Special thanks to Luis G. V. Gonçalves and Jose P. Rino, from UFSCar Physics Department, Brazil for performing time-consuming MD simulations at our request, which shed some light into the diffusivities of the ionic species in LS_2 glass at high temperatures.

APPENDIX A: ANALYSIS OF THREE PHENOMENA THAT COULD AFFECT DIFFUSION COEFFICIENTS

A decoupling between viscous flow and crystal nucleation and growth at T_d was clearly shown by our analysis of the temperature dependence of the several diffusion coefficients. To reinforce these findings, we will discuss some factors (*metastable phase formation*, *internal stresses, or crystal morphology changes*) that could, in principle, affect the above conclusions. We will analyze some parameters that appear in the equations employed for estimation of the diffusion coefficients. Fortunately, in Eqs. (30) and (7), repeated below as Eqs. (A2) and (A1), respectively, for clarity, mainly the thermodynamic driving force $\Delta G \equiv \Delta G_V V_m$ can differ from the values used in our calculations if, for instance, metastable phases or internal elastic stresses affect crystal growth.

$$\tau_S = \frac{80}{3}\frac{k_B T \gamma}{\Delta G_V^2 \lambda^2 D_\tau}, \tag{A1}$$

$$U = D_U \frac{\Delta G}{4\pi \gamma V_M}\left[1 - \exp\left(-\frac{\Delta G}{RT}\right)\right]. \tag{A2}$$

We will discuss below the possible influence of $\Delta G \equiv \Delta G_V V_m$ for the two possibilities above described.

1. Effect of metastable phases

The eventual formation of a metastable or an intermediate phase in the early stage of phase transformation in LS_2 glass was intensively studied and discussed by several authors (see, e.g., Refs. 109–111. In the present case, this possibility could affect only the effective diffusion coefficient D^{τ}_{eff} estimated from the nucleation time-lags because the crystal growth rates refer to macro-crystals of lithium disilicate, the stable phase. By definition, the thermodynamic driving force for the formation of any metastable phase is *lower* than that of the stable phase. Therefore, if the measured nucleation rates refer to a metastable phase, the theoretical value of ΔG_V should be reduced. This reduction would result in an increase of D^{τ}_{eff} estimated from Eq. (7), thus *reinforcing* the difference between D^{τ}_{eff} and D^{η}_{eff} (see Fig. 10). Moreover, because, according to Turnbull[112] and Skapski,[113] a reduction of ΔG_V is always accompanied by a decrease in γ ($\gamma \sim \Delta H_m$), the effect of the eventual formation of metastable phases on the estimation of D^{τ}_{eff} will be weaker.

2. Effect of elastic stresses

Elastic stresses caused by the difference in the specific volume of the liquid and crystalline phases could, in certain conditions, slow the crystallization kinetics. Crystallization governed by the diffusion of building units is responsible for stress production, while stress relaxation is determined by viscous flow. As long as the SEE equation holds, elastic stresses should not have any effect on crystal nucleation and growth. However, below the temperature of decoupling of diffusion and viscous flow, when the SEE equation breaks down, stresses may have a significant influence on crystal nucleation and growth. The origin of this influence consists of a reduction of the thermodynamic driving force for crystallization due to the energy of the residual stresses, which did not relax during the characteristic time (see more details, e.g., in Refs. 77 and 114–116). With respect to our problem, such reduction of ΔG_V would result in an increase of both D^{τ}_{eff} and D_U estimated via Eqs. (7) and (30), respectively, reinforcing the decoupling effect.

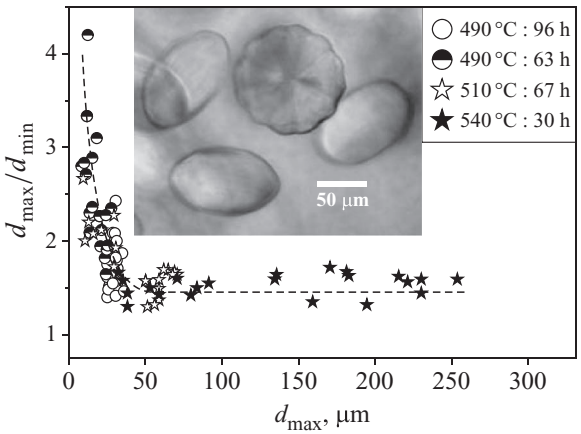

FIG. 13. Ratio between the maximal and minimal diameters of lithium disilicate crystals versus maximal diameter for different heat treatment temperature. The inset shows different morphologies of lithium disilicate crystals grown at 600 °C (Ref. 84).

3. Effect of crystal morphology changes

We should also make a few comments on the crystal morphology in connection with crystal growth rates and with the D_U values. In a wide temperature range the LS_2 crystals grow as ellipsoids of revolution with internal radiant spherulitic structure. The ratio between the maximum and minimum diameters $K = d_{max}/d_{min}$ varies with temperature and crystal size. Fig. 13 shows a trend of increasing K with decreasing temperature and crystal size d_{max}. It should be emphasized that, regardless of the crystal form, the crystal growth rates at a given temperature in the direction of the maximal size are the same as the growth rate of the crystalline layer. For example, one can see in the inset photo in Fig. 13 that the maximal sizes of crystals with the form of ellipsoid of revolution (d_{max}) and sphere (d) are similar (see more details in Ref. 77). Thus, employing the maximal growth rates for our analysis, we get the correct temperature dependence of $U(T)$. Moreover, taking into account that K varies not more than fivefold, it is clear that any change of crystal form cannot appreciably affect D_U as compared with its exponential temperature dependence.

Thus, none of the above possibilities—nucleation of a metastable phase as the first crystalline phase, the influence of elastic stresses at the lowest temperatures and changes of

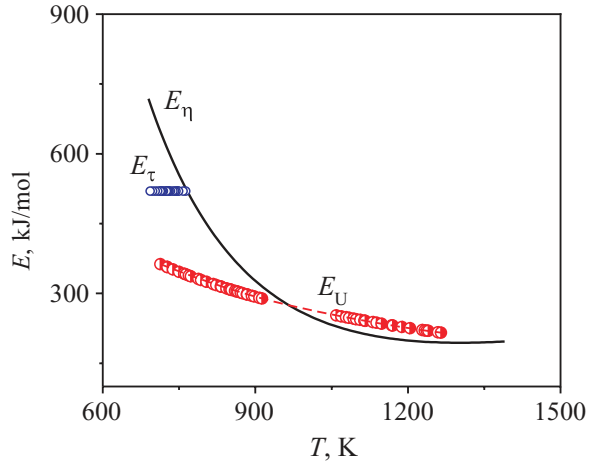

FIG. 14. Activation enthalpies for viscous flow, crystal growth, and nucleation time-lags.

crystal morphology—cannot eliminate the observed decoupling effects, and the provided evidences for the breakdown of the SEE equation are solid.

APPENDIX B: ACTIVATION ENTHALPIES AS A FUNCTION OF TEMPERATURE FOR SEVERAL TYPES OF TRANSPORT PROCESSES

Fig. 14 shows the activation enthalpy, E, of three transport processes studied in the present paper: viscous flow, crystal growth, and crystal nucleation (to be more exact, of their kinetic part). One can see that, at high temperatures, E for viscous flow (taken from Eq. (2)) practically matches that for crystal growth, indicating the validity of the SEE equation. However, at low temperatures ($T < T_d^U$), decoupling of these two processes occurs. Data for the time-lag for nucleation is available only in a narrow temperature interval near the glass transition temperature T_g, where decoupling of nucleation and viscous flow is clearly observed.

APPENDIX C: PRE-EXPONENTIAL PARAMETERS AND ACTIVATION ENTHALPIES (E_A) FOR DIFFERENT DIFFUSION PROCESSES IN LS_2 LIQUID AND GLASS

To facilitate the use of the data presented in the present paper, we collected pre-exponential parameters and activation enthalpies (E_A) for ionic conduction, viscous flow, and ionic and effective diffusion determined from different methods in Table I. Considering activation enthalpies determined from different methods, we can make a few comments about Table I. Is possible to note that below T_g, enthalpies for ionic conductivities (63 ± 1 kJ/mol) are close to the enthalpy of lithium self-diffusion (75 ± 1 kJ/mol) measured by Beier and Frischat.[58] While the oxygen self-diffusion enthalpies are higher than those for lithium below T_g, only one of them is too high.[59] Inter-diffusion enthalpies for Li-Si are similar to calculated values for D_{eff}^{η}, as shown in Fig. 10 and Table I. The diffusional processes for viscous flow, nucleation time-lags and crystal growth shown in Fig. 10 and listed in Table I show that the first ones presented similar activation enthalpies (511–521 kJ/mol), which are higher than the last (342

TABLE I. Pre-exponential parameters and activation enthalpies (E_A) for ionic conduction, viscous flow, and ionic and effective diffusion coefficients determined by different methods.

Mechanism	Equation	Method	ΔT range (K)	Pre-exponential factor	E_A (kJ/mol)	Reference
Ionic conduction	$\sigma T = A_\sigma \exp(-\frac{E_A^\sigma}{RT})$	Arrhenius	Below T_g	$A_\sigma = (1.1 \pm 1.4) \times 10^5$ K S/cm	$E_A^\sigma = 63 \pm 1$	Fig. 9
Ionic conduction	$\sigma T = A_\sigma^* \exp(-\frac{E_A^*}{RT}) \exp[-\frac{B_\sigma}{R(T-T_0)}]$	DML	T_g–T_m	$A_\sigma^* = (1.1 \pm 1.4) \times 10^5$ K S/cm	$E_A^* = 46 \pm 1$ ($B_\sigma = 4.0 \pm 0.2$)	Fig. 9
D^{Li}: Beier and Frischat	$D^{Li} = D_0^{Li} \exp(-{}^{Li}E_A^D/RT)$	Ion diffusion exchange	543–723	$D_0^{Li} = 2.44 \times 10^{-6}$ m^2/s	${}^{Li}E_A^D = 75 \pm 1$	Ref. 58
D^O: Sakai *et al.*	$D^O = D_0^O \exp(-{}^OE_A^D/RT)$	Ion diffusion exchange	598–663	$D_0^O = 2.9 \times 10^{-12}$ m^2/s	${}^OE_A^D = 121 \pm 14$	Ref. 59
D^O: Takizawa *et al.*	$D^O = D_0^O \exp(-{}^OE_A^D/RT)$	Ion diffusion exchange	623–723	$D_0^O = 1.33 \times 10^{-14}$ m^2/s	${}^OE_A^D = 86 \pm 5$	Ref. 60
$D^{Li\text{-}Si}$: Kawakami *et al.*	$D^{Li-Si} = D_0^{Li-Si} \exp(-{}^{Li-Si}E_A^D/RT)$	Interdiffusion Li-Si	1373–1623	$D_0^{Li-Si} = 7.2 \times 10^{-7}$ m^2/s	${}^{Li-Si}E_A^D = 138 \pm 7$	Ref. 61
Viscous flow	$\eta = A_\eta^* \exp[\frac{B_\eta^*}{R(T-T_0)}]$	VFTH	T_g–T_m	$A_\eta^* = 2.176 \times 10^{-3}$ Pa s	$B_\eta^* = 65.72 \pm 0.57T_0 = 490.7$ K	Fig. 1
Diffusion by viscous flow	$D_\eta = D_0 \exp(-E_A^\eta/RT)$	Viscous flow/Arrhenius	718–820	$D_0 = 1.21 \times 10^{16}$ m^2/s	$E_A^\eta = 521 \pm 16$	Fig. 10
Diffusion by time-lag	$D_{\tau_S} = D_{\tau_0} \exp(-E_A^\tau/RT)$	Induction time/Arrhenius	693–763	$D_{\tau_0} = 1.74 \times 10^{14}$ m^2/s	$E_A^\tau = 511 \pm 14$	Fig. 10
Diffusion by crystal growth	$D_U = D_0 \exp(-E_A^U/RT)$	Growth/Arrhenius	713–817	$D_0 = 6.131 \times 10^4$ m^2/s	$E_A^U = 341.6 \pm 9.7$	Fig. 10

± 10 kJ/mol). This finding also indicates the breakdown of SEE relation in the temperature range considered (near-T_d to T_g).

[1] E. D. Zanotto, Am. Ceram. Soc. Bul. **89**, 19 (2010).
[2] J. W. P. Schmelzer, in *Nucleation Theory and Applications*, edited by J. W. P. Schmelzer, G. Röpke, and V. B. Priezzhev (Joint Institute for Nuclear Research Publishing Department, Dubna, Russia, 1999), p. 1.
[3] V. M. Fokin, E. D. Zanotto, N. S. Yuritsyn, and J. W. P. Schmelzer, J. Non-Cryst. Solids **352**, 2681 (2006).
[4] M. Ito, T. Sakaino, and T. Moriya, Bull. Tokyo Inst. Technol. **88**, 127 (1968).
[5] V. N. Filipovich and A. M. Kalinina, Izv. Akad. Nauk. SSSR, Ser. Neorg. Mater. **4**, 1532 (1968) (in Russian).
[6] J. O. M. Bockris, J. D. Mackenzie, and J. A. Kitchener, Trans. Faraday Soc. **51**, 1734 (1955).
[7] Kh. El-Badry, N. A. Ghoneim, H. A. El-Batal, M. M. Ammar, and S. Gharib, Sprechsaal **114**, 599 (1981).
[8] V. M. Fokin, A. M. Kalinina, and V. N. Filipovich, J. Cryst. Growth **52**, 115 (1981).
[9] C. J. R. Gonzalez-Oliver, Ph.D. dissertation, University of Sheffield, UK, 1979.
[10] M. R. Heslin and J. E. Shelby, Proceedings of the XVI International Congress on Glass, Bol. Soc. Esp. Ceram. Vid. 31-C, Madrid (1992), p. 95.
[11] B. A. Marcheschi, M.Sc. thesis, Alfred University, 1985.
[12] R. Ota, F. Tsuchiya, K. Kawamura, Sh. Nakanishi, and J. Fukunaga, J. Ceram. Soc. Jpn. **99**, 168 (1991).
[13] L. Shartsis, S. Spinner, and W. Capps, J. Am. Ceram. Soc. **35**, 155 (1952).
[14] A. I. Vasiliev and A. A. Lisenenkov, in *Proizvodstvo i Issledovanie Stekla i Silikatnykh Materialov* (Verkhne-Volzhskoe Knizhnoe Izd., Yaroslavl, 1978), p. 144 (in Russian).
[15] B. M. Wright and J. E. Shelby, Phys. Chem. Glasses: Eur. J. Glass Sci. Technol. B **41**, 192 (2000).
[16] Z. Zeng, J. Chin. Silic. Soc. **14**, 347 (1986).
[17] T. Izumitani and Y. Moriya, J. Ceram. Assoc. Jpn. **70**, 131 (1962).
[18] I. Joseph, Ph.D. dissertation, Alfred University, USA, 1985.
[19] K. Matusita, M. Koide, and T. Komatsu, J. Non-Cryst. Solids **140**, 141 (1992).
[20] L. L. Burgner and M. C. Weinberg, J. Non-Cryst. Solids **279**, 28 (2001).
[21] V. M. Fokin, N. S. Yritsin, O. V. Potapov, B. A. Shakhmatkin, N. M. Vedisheva, V. L. Ugolkov, and A. G. Cherepova, Russ. J. Phys. Chem. A **77**, 146 (2003).
[22] C. J. R. Gonzalez-Oliver, P. S. Johnson, and P. F. James, J. Mater. Sci. **14**, 1159 (1979).
[23] K. Matusita and M. Tashiro, J. Ceram. Assoc. Jpn. **81**, 500 (1973).
[24] T. Ogura, R. Hayami, and M. Kadota, J. Ceram. Assoc. Jpn. **76**, 277 (1968).
[25] R. Ota and J. Fukunaga, *Proceedings of the XVth International Congress on Glass, Leningrad* (Nauka, Moscow, 1989), Vol. 1a, p. 162.
[26] A. Schmidt and G. H. Frischat, Phys. Chem. Glasses: Eur. J. Glass Sci. Technol. B **38**, 161 (1997).
[27] P. C. Soares, Jr., Ph.D. dissertation, Federal University of São Carlos, Brazil, 2002 (in Portuguese).
[28] E. D. Zanotto and M. L. G. Leite, J. Non-Cryst. Solids **202**, 145 (1996).
[29] M. G. Degen and N. A. Toropov, Izv. Akad. Nauk. SSSR, Ser. Neorg. Mater. **2**, 1617 (1966).
[30] E. D. Zanotto, Ph.D. dissertation, University of Sheffield, 1982.
[31] K. Matusita and M. Tashiro, J. Non-Cryst. Solids **11**, 471 (1973).
[32] M. F. Barker, Tian-He Wang, and P. F. James, Phys. Chem. Glasses **29**, 240 (1988).
[33] J. Deubener, R. Brückner, and M. Sternitzke, J. Non-Cryst. Solids **163**, 1 (1993).
[34] P. F. James, Phys. Chem. Glasses **15**, 95 (1974).
[35] A. A. Leontjeva, in *Soveshchanie po Vyazkosti Zhidkostei i Kolloidnykh Rastvorov, Moskva*, edited by M. P. Volarovich (Akad. Nauk. SSSR, Institute of Machine Science, Moscow, 1945), Vol. 3, p. 70.
[36] D. Parcell, Ph.D. dissertation, University of Florida, 1993.
[37] V. Brätsch and G. H. Frischat, J. Non-Cryst. Solids **95–96**, 457 (1987).
[38] V. N. Filipovich and A. M. Kalinina, Izv. Akad. Nauk. SSSR, Ser. Neorg. Mater. **7**, 1844 (1971).
[39] V. M. Fokin, Ph.D. dissertation, Silicate Chemistry Institute, Leningrad, 1980 (in Russian).
[40] G. A. Sycheva, Glass Phys. Chem. **24**, 342 (1998).
[41] J. J. Tuzzeo, Ph.D. dissertation, Ohio State University, USA, 1976.
[42] Z. Zeng, J. Chin. Silic. Soc. **15**, 122 (1987).
[43] E. G. Rowlands and P. F. James, Phys. Chem. Glasses **20**, 1 (1979).
[44] J. O. M. Bockris, J. A. Kitchener, S. Ignatowicz, and J. W. Tomlinson, Trans. Faraday Soc. **48**, 75 (1952).
[45] A. E. Dale, E. F. Pegg, and J. E. Stanworth, J. Soc. Glass Technol. **35**, 136 (1951).
[46] M. Hahnert, A.-R. Grimmer, and D. Kruschke, *Proceedings of the XVth International Congress on Glass, Leningrad* (Nauka, Moscow, 1989), Vol. 1a, p. 149.
[47] P. L. Higby and J. E. Shelby, J. Am. Ceram. Soc. **67**, 445 (1984).
[48] A. Kone, B. Barrau, J.-L. Souquet, and M. Ribes, Mater. Res. Bull. **14**, 393 (1979).
[49] K. A. Kostanyan and E. A. Erznkyan, Arm. Khim. Zh. **20**, 358 (1967).
[50] V. K. Leko, Izv. Akad. Nauk. SSSR, Ser. Neorg. Mater. **3**, 1224 (1967).
[51] O. V. Mazurin and E. S. Borisovskii, Zh. Tekh. Fiz. **27**, 275 (1957).
[52] O. V. Mazurin and V. A. Tsekhomskii, Izv. Vyssh. Uchebn. Zaved. Fiz. (Tomsk) **1**, 125 (1964).
[53] A. A. Pronkin, Glass Phys. Chem. **5**, 634 (1979).
[54] J.-L. Souquet, A. Kone and M. Ribes, J. Non-Cryst. Solids **38–39**, 307 (1980).
[55] V. I. Vakhrameev, Steklo **3**, 84 (1968).
[56] M. Yoshiyagawa and M. Tomozawa, Solid State Ionics **23**, 271 (1987).
[57] A. A. Campos-Junior and A. C. M. Rodrigues, J. Appl. Phys. **100**, 053709 (2006).
[58] W. Beier and G. H. Frischat, J. Non-Cryst. Solids **38–39**, 569 (1980).
[59] T. Sakai, K. Takizawa, T. Eguchi, and J. Horie, J. Mater. Sci. Lett. **14**, 1126 (1995).
[60] K. Takizawa, T. Sakai, and K. Ohishi, J. Chem. Soc. Jpn. **9**, 1522 (1981).
[61] M. Kawakami, K. Nagata, and K. S. Goto, J. Electrochem. Soc. **125**, 395 (1978).
[62] L. Battezzati, M. Kusý, M. Palumbo, and V. Ronto, *Properties and Applications of Nanocrystalline Alloys from Amorphous Precursors*, NATO Science Series, edited by B. Idzikowski, P. Svec, and Y. Marcel (Kluwer, Dordrecht, 2005), Vol. 184, p. 267.
[63] S. M. Chathoth and K. Samwer, Appl. Phys. Lett. **97**, 221910 (2010).
[64] K. L. Ngai, J. H. Magill, and D. J. Plazek, J. Chem. Phys. **112**, 1887 (2000).
[65] M. D. Ediger, P. Harrowell, and Lian Yu, J. Chem. Phys. **128**, 034709 (2008).
[66] M. K. Mapes, S. F. Swallen, M. D. Ediger, J. Chem. Phys. B **110**, 507 (2006).
[67] F. Mallamace, C. Corsaro, H. E. Stanley, and S.-H. Chen, Eur. Phys. J. E **34**, 94 (2011).
[68] S. C. Glotzer, J. Non-Cryst. Solids **274**, 342 (2010).
[69] J. Deubener, R. Muller, H. Behrens, and G. Heide, J. Non-Cryst. Solids **330**, 268 (2003).
[70] M. L. F. Nascimento, Ph.D. dissertation, Federal University of São Carlos, Brazil, 2005.
[71] I. Gutzow and J. W. P. Schmelzer, *The Vitreous State* (Springer, Berlin, 1995).
[72] H. Vogel. Phys. Z. **22**, 645 (1921).
[73] G. S. Fulcher, J. Am. Ceram. Soc. **8**, 339 (1925).
[74] G. Tammann, W. Hesse, and Z. Anorg. Allg. Chem. **156**, 245 (1926).
[75] J. C. Mauro, Y. Yue, A. J. Ellison, P. K. Gupta, and D. C. Allana, Proc. Natl. Acad. Sci. U.S.A. **106**, 19780 (2009).
[76] I. Avramov and A. Milchev, J. Non-Cryst. Solids **104**, 253 (1988).
[77] J. W. Christian, *The Theory of Transformations in Metals and Alloys. Part I* (Pergamon, Oxford, UK, 1981).
[78] A. A. Cabral, V. M. Fokin, E. D. Zanotto, and C. R. Chinaglia, J. Non-Cryst. Solids **330**, 174 (2003).
[79] V. V. Slezov, *Kinetics of First-Order Phase Transitions* (Wiley VCH, Berlin, 2009).
[80] F. C. Collins, Z. Electrochem. **59**, 404 (1955).
[81] D. Kashchiev, Surf. Sci. **14**, 209 (1969).
[82] G. Tammann, Z. Phys. Chem. **25**, 441 (1898).
[83] Sciglass® 6.5 database, Institute of Theoretical Chemistry, Shrewsbury, 2005.
[84] V. M. Fokin, A. A. Cabral, R. M. C. V. Reis, M. L. F. Nascimento, and E. D. Zanotto, J. Non-Cryst. Solids **356**, 358 (2010).
[85] A. M. Kalinina, V. N. Filipovich, V. M. Fokin, and G. A. Sycheva, in *Proceedings of the XIVth International Congress on Glass*, New Delhi (1986), Vol. 1, p. 366.

[86]M. L. F. Nascimento and E. D. Zanotto, Phys. Rev. B **73**, 024209 (2006).
[87]M. L. F. Nascimento and E. D. Zanotto, Phys. Chem. Glasses: Eur. J. Glass Sci. Technol. B **48**, 201 (2007).
[88]I. Gutzow, in *Crystal Growth and Materials*, edited by E. Kaldis and H. J. Scheel (North-Holland, Amsterdam, 1977).
[89]D. R. Uhlmann, E. V. Uhlmann, and M. C. Weinberg, *Nucleation and Crystallization in Liquids and Glasses* (The American Ceramic Society, Westerville, OH, 1993).
[90]M. L. F. Nascimento, E. B. Ferreira, and E. D. Zanotto, J. Chem. Phys. **121**, 8924 (2004).
[91]V. M. Fokin, J. W. P. Schmelzer, M. L. F. Nascimento, and E. D. Zanotto, J. Chem. Phys. **126**, 234507 (2007).
[92]M. L. F. Nascimento and E. D. Zanotto, J. Chem. Phys. **133**, 174701 (2010).
[93]A. S. Skapski, J. Chem. Phys. **16**, 386 (1948).
[94]D. Turnbull, J. App. Phys. **21**, 1022 (1950).
[95]K. A. Jackson, in *Growth and Perfection of Crystals*, edited by R. H. Doremus, B. W. Roberts, and D. Turnbull (Wiley, New York, 1958).
[96]K. Takahashi and T. Yoshio, J. Ceram. Soc. Jpn. **81**, 524 (1973).
[97]J.-L. Souquet, M. L. F. Nascimento, and A. C. M. Rodrigues, J. Chem. Phys. **132**, 034704 (2010).
[98]G. J. Dienes, J. Appl. Phys. **24**, 779 (1953).
[99]P. B. Macedo and T. A. Litovitz. J. Chem. Phys. **42**, 245 (1965).
[100]J.-L. Souquet, M. Duclot, and M. Levy, Solid State Ionics **105**, 237 (1998).
[101]M. L. F. Nascimento, A. C. M. Rodrigues, and J.-L. Souquet, Phys. Chem. Glasses: Eur. J. Glass Sci. Technol. B **51**, 69 (2010).
[102]L. G. V. Gonçalves and J. P. Rino, e-print arXiv:1107.0760v1 [cond-mat.mtrl-sci].
[103]J. W. P. Schmelzer, R. Muller, J. Moller, and I. S. Gutzow, J. Non-Cryst. Solids **315**, 144 (2003), and references cited therein.
[104]V. M. Fokin and E. D. Zanotto, J. Non-Cryst. Solids. (unpublished).
[105]H. Sillescu, J. Non-Cryst. Solids **243**, 81 (1999).
[106]M. D. Ediger, Annu. Rev. Phys. Chem. **51**, 99 (2000).
[107]H. Tanaka, Phys. Rev. E **68**, 011505 (2003).
[108]J. Schneider, V. R. Mastelaro, E. D. Zanotto, B. A. Shakhmatkin, N. M. Vedishcheva, A. C. Wright, and H. Panepucci, J. Non-Cryst. Solids **325**, 164 (2003).
[109]Y. Iqbal, W. E. Lee, D. Holland, and P. F. James, J. Non-Cryst. Solids **224**, 1 (1998).
[110]L. L. Burgner, P. Lucas, M. C. Weinberg, P. C. Soares, Jr., and E. D. Zanotto, J. Non-Cryst. Solids **274**, 188 (2000).
[111]P. C. Soares, Jr., E. D. Zanotto, V. M. Fokin, and H. Jain, J. Non-Cryst. Solids **331**, 217 (2003).
[112]D. Turnbull, J. Chem. Phys. **18**, 769 (1950).
[113]A. S. Skapski, Acta Metall. **4**, 576 (1956).
[114]J. W. P. Schmelzer, O. V. Potapov, V. M. Fokin, R. Muller, and S. Reinsch, J. Non-Cryst. Solids **333**, 150 (2004).
[115]J. W. P. Schmelzer, E. D. Zanotto, I. Avramov, and V. M. Fokin, J. Non-Cryst. Solids **352**, 434 (2006).
[116]V. M. Fokin, E. D. Zanotto, J. W. P. Schmelzer, and O. V. Potapov, J. Non-Cryst. Solids **351**, 1491 (2005).